Optimisation of PtxNiyAlz ratios as thin film electrocatalysts for the oxygen evolution reaction (OER) in alkaline medium

HK Kishinkwa

orcid.org 0000-0003-3805-9991

Dissertation accepted in partial fulfilment of the requirements for the degree *Master of Science in Chemistry* at the North-West University

Supervisor: Prof RJ Kriek

Co-supervisor: Dr A Falch

Graduation October 2020

23692979

ACKNOWLEDGEMENTS

“For I know the plans I have for you.” Declares the **LORD**, “Plans to **PROSPER** you and not to harm you. Plans to give you **HOPE** and a **FUTURE**.” – **Jeremiah 29:11**

Firstly, I would like to give thanks and praises with a humble and grateful heart to my heavenly Father for giving me life, sustaining me and abundantly blessing me.

My sincere gratitude goes to the following people:

- My loving husband Katlego Khobo. Your undying love and support have carried me through this degree and always gave me reason to not give up. I bless the day you came into my life.

- My family and friends for their continuous support and encouragement. Your love that kept me going and mostly for the vote of confidence that kept me motivated.

- Dr Boitumelo Mogwase and Dr Zafar Iqbal for the help, assistance and guidance throughout this project. You made me love Electrochemistry.

- To my supervisor Prof RJ Kriek and my co-supervisor Dr A Falch, my sincere gratitude extends to you for your support and guidance throughout this project

Lastly, I would like to acknowledge Lonmin for the bursary awarded to me for this research project and the Chemical Resource Beneficiation (CRB) research focus area of the North-West University (Potchefstroom Campus) for funding of laboratory chemicals and equipment.

****Dedicated to my son Khumo Nathan Khobo****

PREFACE

I (Huguette Kaganda Kishinkwa), declare that the following dissertation is submitted in article format as is allowed by the North-West University (NWU). This means that the conventional dissertation structure will be followed for the background and motivation (Chapter 1), Literature review (Chapter 2). The experimental, results and discussion chapter is excluded because this information is contained in the article. The article will form part of Chapter 3. Consequently, the repetition of certain information will occur.

ABSTRACT

The world is currently reliant on energy sources such as oil, coal and gas (all fossil fuels) for the supply of the global growing energy demand. However, these fossil fuels are diminishing and have drawbacks such as the constant emission of carbon dioxide (CO_2) to the atmosphere. Research seeking alternative energy technologies, based on renewable energy resources, has identified hydrogen gas (H_2) as a clean energy carrier. Alkaline water electrolysis (AWE) is one of the most preferred and advantageous techniques for clean hydrogen gas (H_2) production. With the efficiency of this technique linked to the activity of the oxygen evolution reaction (OER) at the anode, the electrochemical production of the hydrogen needs to be optimised due to the sluggish kinetics and large overpotentials of the OER. This has resulted in the search for OER electrocatalysts that allow for high electrocatalytic activity and stability under harsh conditions. IrO_2 and RuO_2 have been identified as the most active OER catalysts in acidic medium for water electrolysers as they produce high current densities at low overpotentials, however these noble metals are costly. Research seeking to identify an efficient and cost-effective AWE electrocatalyst that can operate at low overpotential with higher current densities and have low noble metal content has shown that Ni and Ni-Al (also known as Rayney Nickel) combinations exhibit excellent activity and stability in alkaline environment for the OER. In this study, combinations of $Pt_xNi_yAl_z$ as thin film electrocatalysts were produced on Si/SiO_2-wafers and glassy carbon supports with magnetron sputtering (PVD) and screened using a high-throughput equipment for analysis. The 10 most promising $Pt_xNi_yAl_z$ were further subjected to electrochemical testing in a three-electrode cell connected to a rotating disc electrode for electrocatalytic activity and short-term stability. Linear sweep voltammetry and chronopotentiometry are the two electrochemical techniques that were employed to determine the electrocatalytic activity and stability. Scanning electron microscopy coupled with energy dispersive X-ray spectroscopy was employed for physical and stoichiometric characterisation of the thin film electrocatalysts. It was found that Pt and Al alone compared to the ternary combinations $Pt_xNi_yAl_z$ are poor electrocatalysts towards the OER, they suffered from stability issues due to the dissolution in the alkaline electrolyte. However, various $Pt_xNi_yAl_z$ exhibited an increase in activity subsequent to the stability testing. The ratios with the highest electrocatalytic activity and stability towards the alkaline OER are $Pt_{12}Ni_{88}$, $Pt_{21}Ni_{47}Al_{32}$ and $Pt_{21}Ni_{54}Al_{25}$ requiring an overpotential of 335 mV, 337 mV and 337 mV to attain a current density of 10 $mA.cm^{-2}$ at 25 °C (subsequent to stability tests). $Pt_{21}Ni_{47}Al_{32}$ and $Pt_{21}Ni_{54}Al_{25}$ also exhibited the lowest Tafel slope values of 46.87 $mV.dec^{-1}$ and 46.46 $mV.dec^{-1}$ respectively. However, the most optimal electrocatalyst is $Pt_{14}Ni_{52}Al_{34}$, as it's the ternary electrocatalyst with the lowest mass of Pt and Ni loading, exhibiting a low overpotential (350 mV) and the lowest Tafel slope (46.46 $mV.dec^{-1}$) after the binary $Pt_{12}Ni_{88}$ subsequent to durability testing. This electrocatalyst exhibits the highest mass specific activity per Pt and Ni loading compared to the

other sputtered electrocatalysts both before and after durability testing. It was concluded that aa combination of Pt, Ni and Al does increase the electroactivityof the catalysts towards the OER. The electrolytic activity of these electrocatalysts was attributed to the higher percentage of Ni content in the electrocatalyst and a lower percentage of Al (which has a leaching property that results in more electroactive surface area).

Keywords: Oxygen evolution reaction (OER), Platinum, Nickel, Aluminium, Activity, Stability

TABLE OF CONTENTS

LIST OF TABLES

LIST OF FIGURES

LIST OF ABBREVIATIONS AND SYMBOLS

Symbol/Abbreviation	Description	unit
i_0	Exchange current density	mA.cm^{-2}
i_k	Kinetic current density	mA.cm^{-2}
i_{lim}	Limiting current density	mA.cm^{-2}
i_f	Current density of forward scan	mA.cm^{-2}
i_b	Current density of backward scan	mA.cm^{-2}
A	Electrode area	cm^2
Ir	Iridium	
C	Concentration	mol.L^{-1}
CP	Chronopotentiometry	
CE	Counter electrode	
CV	Cyclic voltammogram	
D_0	Diffusion coefficient	cm^2.s^{-1}
DFT	Density functional theory	
e-	Electron	
E^0	Standard electrode potential	V
E_{LOW}	Lower potential value	
F	Faraday's constant	C.mol^{-1}
H^+	Proton	
H_2	Hydrogen	
H_2O	Water	

K-L	Koutecky-Levich	
KOH	Potassium Hydroxide	
LSV	Linear sweep voltammetry	
n	Number of Electrons	
O_2	Oxygen	
OH-	Hydroxide	
ORR	Oxygen reduction reaction	
OER	Oxygen evolution reaction	
PEM	Proton exchange membrane	
Pt	Platinum	
Ni	Nickel	
Al	Aluminium	
R	Ideal gas constant	$J.K^{-1}.mol^{-1}$
RDE	Rotating Disk Electrode	
RE	Reference electrode	
Ru	Ruthenium	
RHE	Reversible hydrogen electrode	
SHE	Standard hydrogen electrode	
T	Temperature	K
WE	Working electrode	
XRD	X-Ray diffraction	
ν	Kinematic viscosity	$cm.s^{-1}$
α	Transfer coefficient	

η	Overpotential	V
η_Ω	Overpotential compensated by resistance of cell	
ω	Rotation rate	s^{-1}
θ	Coverage by an adsorbate	
EDX	Energy dispersive X-ray spectroscopy	
SEM	Scanning electron microscopy	
ν	Scan rate	
ECSA	Electrochemical active surface area	
q^*	Volumetric charge	
ZIR	Impedance measurement technique	
R	Ohmic resistance of cell	Ω

1 INTRODUCTION

This chapter serves as an introduction to the general theme of the dissertation, which includes a summary (substantiated by a brief literature overview), aim and objectives, research methodology and dissertation overview.

It is kindly requested to note that this dissertation is in article format, the literature research referred to in the following sections of Chapter 1 and 2 are in addition to the literature used in the introduction of the article listed in Chapter 3; in this regard repetition of information could occur.

1.1 Background

1.1.1 Energy

The global demand for energy has drastically increased in the past decade, and is expected to escalade in the next coming years according to the International Energy Agency (IEA), which is due to the continuous growth in the world's population as well as the progressive industrialisation of developing nations around the world [1]. The estimated global population has increased to approximately 7.8 billion over the past 200 years and has resulted in a drastic increase in the demand for energy [2]. In 2018 global energy consumption increased at twice the average growth-rate since 2010, which was attributed to the robust global economy and higher heating and cooling needs in different parts of the world. The demand for all fuel types as source of energy has drastically increased with natural gas leading as fuel of choice, which accounts for nearly 45% of the increase in total energy demand in 2018. Although the use of renewables has grown at a double-digit pace, it's still not fast enough to meet the high electricity demand that was responsible for over half of the growth in global energy [3]. By 2040, the International Energy Agency (IEA) projects a growth in energy demand of 37%, which will come as a result of a growing population and economy that will be less energy-intensive in comparison to the present situation. It is expected that by 2040, the world's energy supply will still greatly depend on fossil fuels (oil, natural gas and coal) [4], which account for 80% of the world's energy supply. These fossil fuel-based technologies, however, are responsible for the constant emission of carbon dioxide (CO_2) to the atmosphere, which cause environmental problems like global warming and climate change [5]. In 2018, global CO_2 emission levels grew by 1.7% reaching a historic 33.1 Gt of CO_2, which was driven by the high energy demand. In addition to the harmful emission of carbon dioxide and other greenhouse

gasses to the atmosphere, the fear of future shortages of oil, coal and renewable energy (bioenergy) has brought forth an urgent need for alternative and clean(er) energy sources [6].

1.1.2 Hydrogen (energy carrier)

The challenges faced with current energy sources have resulted in the research and development of alternative energy technologies, which are based on renewable energy resources and associated chemical processes [7]. Renewable energy refers to abundant natural resources that can be utilised for sustainable energy supply with the possibility of no harmful bi-products that can negatively impact humans and the environment. To list a few: wind, hydro, solar, photovoltaic, biomass and geothermal power are some of these renewable energies. Research shows that, coupled to right policies and advance technology evolutions, the renewable energy sector could increase from the current 13.5% to 50% by 2050 [8]. During this search hydrogen has been identified as a possible alternative renewable and sustainable energy carrier that responds positively to global economic growth and environmental concerns [9-11]. A clear depiction of hydrogen as being a source of energy for the future is seen in the following illustration (Figure 1.1) depicting the transition of global energy systems [12].

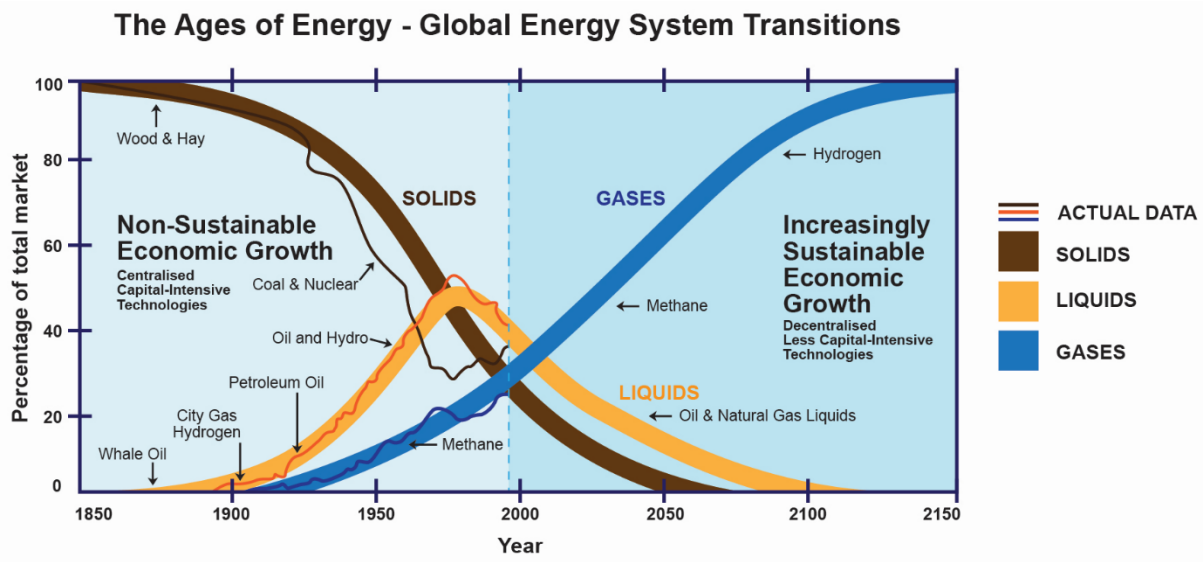

Figure 1.1. Global energy system transition (redrawn from [12])

While hydrogen is the simplest and lightest of all elements, it is the most abundant atom in the universe, making up 75% of the universe's mass [13]. In its molecular form, hydrogen is considered a clean energy carrier that, during processing, i.e. energy release/conversion, emits no by-products (pollutants) other than water [14, 15]. Hydrogen is seen as a suitable alternative to fossil fuels in ensuring sustainable energy supply [16].

Hydrogen can be produced employing ninety different production routes, which can be subdivided into four categories, i.e. biological, chemical, electrochemical and thermal [17]. Natural gases have been used in different methods to produce hydrogen, which account for over 95% of all hydrogen production in the U.S and 48% globally. Currently, steam methane reforming (SMR) is the dominant industrial process used to produce hydrogen, as it offers an efficient and economical process. The SMR process has an efficiency of approximately 65% to 75%, however, the SMR process in centralized plants is not a completely clean process due to its emission of more than twice the amount by mass of CO_2 than the actual amount of hydrogen produced. However, more hydrogen is produced by number of moles than CO_2. Equations 1 – 3 exhibit the multi-steps and conditions associated to the SMR process. In the first reforming step (Eqs. (1) and (2)), methane reacts with steam to form hydrogen and carbon monoxide. These endothermic reactions are carried out at 800-1000 ºC and at 14-20 atm over a Ni-based catalyst. Equation 3 (the net reaction) is an exothermic reaction favoured by low temperatures; this occurs as the reformer products from Eq. 1 and 2 are fed to a water gas shift (WGS) reactor for the separation of hydrogen from the syngas.

$CH_4 + H_2O \rightleftharpoons CO + 3H_2$ $\Delta H^o_{298} = 206.2$ kJ / mol (1)

$CO + H_2O \rightleftharpoons CO_2 + H_2$ $\Delta H^o_{298} = -41.2$ kJ / mol (2)

$CH_4 + 2H_2O \rightleftharpoons CO_2 + 4H_2$ $\Delta H^o_{298} = 165$ kJ / mol (3)

The emission of CO_2 into the atmosphere can be countered using technologies such as carbon capture and sequestration, however, these are new technologies with no long-term evidence of success [18, 19].

Water electrolysis, a promising electrochemical process that has been in the industry for decades, has numerous advantages, which includes the production of high purity hydrogen as well as the possibility of being pollution free (if coupled to wind or solar) [16, 20].
Water electrolysis can be divided into three categories: alkaline water electrolysers, polymer electrolyte membrane (PEM) electrolysers and solid oxide electrolysis.
Alkaline media is mostly preferred with respect to the other water electrolysis methods as it is a well-established method and uses cheaper materials. Additionally, alkaline water electrolysis produces clean hydrogen (purity of 99.99%) and oxygen in comparison to SMR and other reforming reactions (without treatment).
The following reactions occur in alkaline water electrolysis:

At the anode (oxygen evolution reaction, OER)

$4OH^- \rightarrow O_2 + 4e^- + 2H_2O$ ($E° = 0.40V$ vs. SHE) (4)

At the cathode (hydrogen evolution reaction, HER)

$2H_2O^- + 4e^- \rightarrow 2H_2 + 4OH^-$ ($E° = -0.83V$ vs. SHE) (5)

The overall reaction for alkaline water electrolysis [21]

$2H_2O \rightarrow 2H_2 + O_2$ ($E° = -1.23V$ vs. SHE) (6)

Producing hydrogen from water electrolysis, that could potentially be driven by solar or wind sources, has one shortcoming in that the oxygen evolution reaction (OER) limits the efficiency of the process, due to it being the rate-determining step for both alkaline and acidic water electrolysis processes. The OER results in a low energy efficiency, which is caused by its high activation overpotential due to the sluggish nature of the electrode kinetics [22, 23]. It is for this specific reason that water electrolysis is not yet economically feasible to replace the current fossil fuel hydrogen production methods. The overall energy requirement for water electrolysis has to be reduced, which can be brought about by optimising the OER through the development of a more active electrocatalyst material for the anode. Addressing this need will increase hydrogen production while decreasing production costs.

Current OER electrocatalysts consist of IrO_2 and RuO_2 in industrial water electrolysers more specifically in PEM electrolysers i.e. acidic medium [7, 24, 25]. These two electrocatalysts are used because of their low overpotentials, however, they are very expensive and scarce [7, 26, 27]. Nickel and Raney nickel (Ni_xAl_y) are other materials that are used as electrocatalysts as they are less expensive in comparison to iridium or ruthenium [7, 28, 29]. Generally, nickel and its alloys are used as anode material for the alkaline OER as they exhibit good catalytic activity and stability [1]. Studies also show that several binary alloys of nickel such as Pt-Ni exhibit moderate catalytic activity towards the OER [30]. Irrespective of the fact that pure platinum is a very expensive metal, studies have identified it as one of the best electrocatalytic electrode materials for the oxygen reduction reaction (ORR) due its low overpotential [16, 31, 32]. Addition of platinum to oxides has also shown improvement in anode activity, stability and conductivity for alkaline electrolysis [33, 34]. Combinatorial sputtering, an efficient high-throughput approach that investigates observable trends in materials of interest, e.g. electrocatalytic activity [23], is a technique that has been used in earlier work conducted within the Electrochemistry for Energy & Environment Group at the North-West University (NWU), which identified $Pt_9Ni_{56}Al_{35}$ as a promising anode electrocatalyst for the OER. However, the ratio of platinum, nickel and aluminium ($Pt_xNi_yAl_z$) needs to be refined and optimised for the OER in alkaline medium.

1.2 Research methodology

As it is of the utmost importance to obtain high current densities in the electrolyser at the lowest possible overpotential, so as to produce an adequate amount of hydrogen efficiently, the main focus of this study is to refine the $Pt_xNi_yAl_z$ ratio, of vapour deposited thin films of this ternary combination, for the oxygen evolution reaction (OER) in alkaline medium, employing a high throughput combinatorial method.

As stated above, pure platinum is the preferred electrocatalyst for the oxygen reduction reaction (ORR), however it only exhibits moderate activity for the OER. Ni as well as Ni-Al have been investigated for alkaline electrolysis, however, there is no available research on PtNiAl combinations as an electrocatalyst for the OER in alkaline medium. In this study, combinations/ratios of Pt, Ni and Al will be investigated. A comparative study will be conducted related to the different ratios of $Pt_xNi_yAl_z$ in order to obtain an optimum bimetallic or trimetallic catalyst for the OER. Overpotential (at 10 $mA.cm^{-2}$), current densities and Tafel slopes are the three variables that will be determined to compare the effectiveness of the electrocatalysts, since a lower overpotential at high current density is ideal for an effective catalyst. In general, high current densities for a specific electrocatalyst are also an indication of faster reaction kinetics, which is also a factor that is used in optimising the electrocatalyst. The use of Tafel slope analysis will also be employed, which provides information regarding the type of OER mechanism i.e. a two electron or four electron process occurring on the electrocatalyst.

The approach taken in this study is to first conduct a literature study on the individual and combined properties of Pt, Ni and Al related to the OER. This will be done in order to obtain a background on previously used Pt, Ni and Al electrocatalysts for the OER. Once the literature study is complete, an excel sheet will be used for the generation of the $Pt_xNi_yAl_z$ electrocatalytic ratios having (initially) a 10 % stoichiometric ratio difference. Before any sputtering is done, calibration of the sputtering rate of the PVD combinatorial equipment will be conducted for each metal. Photolithography will be employed to develop an electronic circuit on the SiO_2 wafer that will be used for the initial activity testing of the generated ratios. Sputtering of the generated ratios as thin films will be performed on the wafer using combinatorial PVD equipment. The thin-film sputtered ratios will be subjected to high-throughput electrochemical screening to identify the most active x, y, z region(s) (highest current densities, lowest onset potentials). Once the active x, y, z region(s) has been identified, a refinement process will be performed to generate new ratios having a 5% stoichiometric difference, to further zoom into the most active x, y, z region(s). These refined thin-film ratios will again be sputtered onto another wafer for electrocatalytic screening to identify the ten most active $Pt_xNi_yAl_z$ ratios. The

ten most active electrocatalysts will then subsequently be sputtered onto polished GC's (see appendix A) and evaluated for the OER by means of electrochemical techniques such as linear polarization (LSV) for activity and chronopotentiometry (CP) for short-term stability/durability in a three-electrode cell-setup.

1.3 Aim and objectives

The main aim of this research project is to refine the ratio of a vapour deposited $Pt_xNi_yAl_z$ thin film electrocatalyst that exhibits both high activity and acceptable durability for the OER in alkaline medium.

In working towards the abovementioned aim, the objectives for this study include the following:

- conduct a literature review on the historic development and current state-of-the-art of electrocatalysts for the oxygen evolution reaction (OER) for electrolytic hydrogen production,
- determine a number of electrocatalyst ratios ($Pt_xNi_yAl_z$) that will be sputtered as thin films on the SiO_2-wafers,
- prepare SiO_2-wafer based electronic circuits as high-throughput supports for the electrocatalytic screening of vapour deposited thin films,
- sputter the determined $Pt_xNi_yAl_z$ ratios onto the wafer using physical vapour deposition (PVD),
- refine the observed electroactive ratios by generating more ($Pt_xNi_yAl_z$) ratios within the observed x, y, z region and
- identify the ten most electrocatalytically active ($Pt_xNi_yAl_z$) ratios from the refined x, y, z region,
- sputter these ten ratios onto GC's and conduct electrochemical kinetic measurements that will be used to determine the most optimum electroactive catalyst, and
- conduct short-term durability/stability tests on these ten most active electrocatalysts identified.

1.4 Dissertation outline

This dissertation will comprise of the following sections:

Chapter 1: Introduction

This chapter focuses on the following:

- Background
- Energy
- Hydrogen as energy carrier
- Research methodology
- Aim and objectives

Chapter 2: Literature review

This chapter will focus on the literature concerning the following:

- Water electrolysis
- Oxygen evolution reaction
- Mechanism for OER
- Electrocatalysts for OER
- Electrocatalyst development
- Electrochemical techniques

Chapter 3: Article

Chapter 3 will consist of a concept paper that is to be submitted to an international ISI accredited journal for possible publication and will have the following outline:

- Introduction
  The information provided in this section will be similar to that provided in chapter 1 (Introduction) and 2 (Literature study).

- Experimental
  Details regarding the experimental investigation of this study will be contained in this section. A clear description of the steps followed for the photolithography, ratio generation and the combinatorial sputtering and screening will be described in depth. The experimental apparatus, techniques, procedures followed to conduct the electrochemical tests that will reveal the most active and stable electrocatalyst (s) will be thoroughly explored.

- Results and discussion
  In this section, the results obtained from the electrochemical investigations conducted will be critically discussed.

- Conclusion
  Conclusions regarding this research project will be made in this section, i.e. whether or not a refined $Pt_xNi_yAl_z$ thin-film ratio was obtained that is active and durable. Recommendations for future work will be stated, and will be followed by the references.

Chapter 4: Supplementary information

Appendix A

This section will provide a detailed description of the experimental procedure followed.

Appendix B

This section will provide additional results obtained throughout this research project.

2 Literature review

This chapter provides a literature study on water electrolysis in general, the oxygen evolution reaction (OER), electrocatalysts used for the OER (related to platinum, nickel, aluminium and possible combinations thereof), the mechanism of the OER and the role of the electrode surface as well as combinatorial and high-throughput methods. In order to investigate the $Pt_xNi_yAl_z$ electrocatalysts for the OER in alkaline medium, catalytic properties have to be investigated and determined. To that regard, this chapter also provides an overview of catalyst analysis methods and the electrochemical techniques used to determine the activity of the electrocatalyst.

2.1 Water electrolysis

Hydrogen is considered an important energy carrier of the future and may be used instead of fossil fuels with the possibility of no harmful emissions [31, 35]. However, hydrogen is not an energy source and does not occur in nature in any form, it has to be produced employing either renewable or non-renewable sources [7, 14, 18]. Amongst the number of methods that have been developed for the production of hydrogen, water electrolysis (a well-established conventional technology) has been deemed the most practical and mature technology [25, 35-39]. This is due to the fact that water electrolysis is relatively efficient (>70%), it can produce green hydrogen (when coupled to a wind or solar energy source) that can be used with no post-combustion pollutants, and water electrolysis has the capacity to produce hydrogen ranging from a few cm^3/min to thousands of m^3/h [40, 41].

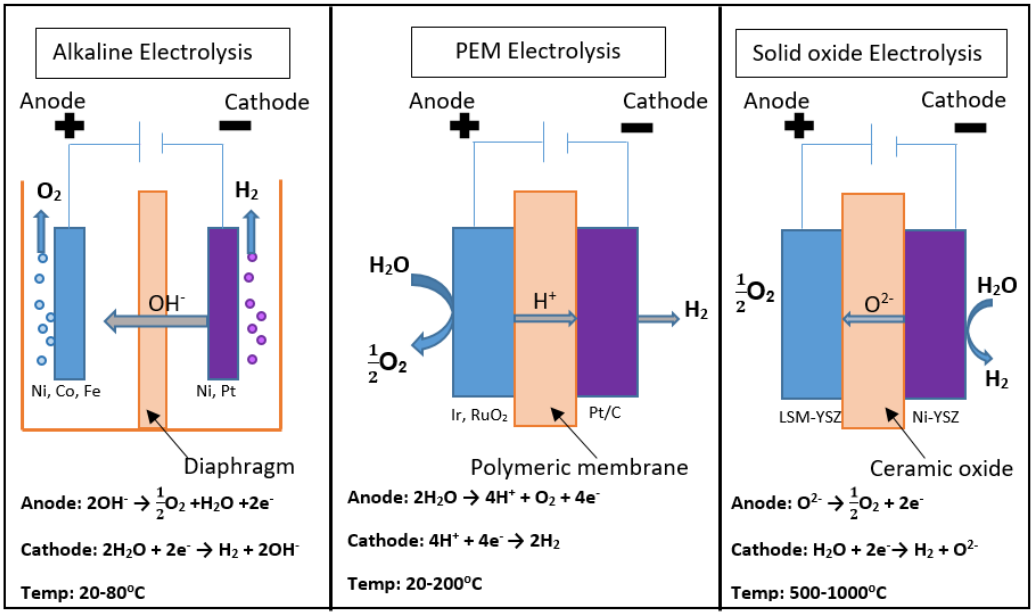

Figure 2.1. Schematic representation of the three types of electrolysis systems, alkaline, PEM proton-exchange membrane) and solid oxide electrolysis as adapted from [7]

Water electrolysers can be divided into alkaline water electrolysers (AWE), polymer electrolyte membrane (PEM) electrolysers, and solid oxide electrolysers (SOE) (Figure 2.1). Although each of these types of water electrolysis methods show promise in sustainable energy applications, they each have their pros and cons. PEM has the advantage that it offers great energy efficiency and high production rates, has a compact design, provides very fast start-up and produces high purity H_2 [7, 35, 40]. The solid state (membrane) of the electrolyte in a PEM allows for a compact design and a dynamic system with a faster response upon application of power supply compared to liquid electrolysers that are susceptible to slow diffusion rates. PEM electrolysers typically operate at low temperatures where water is liquid, however, fuel cell technology is progressing in that polymeric membrane are developed that can operate up to 200 °C, which could also find application in PEM electrolysers. The main inhibitors for the commercialization of PEM electrolyser technology include the high cost of the polymeric membranes and noble metal electrocatalysts (e.g. IrO_2 and RuO_2) as well as the material for the bipolar plates [7, 27, 42]. The SOE, which operates at high temperatures (500 – 1 000 °C) compared to low temperature electrolysers, provides enhanced kinetics, thermodynamics as well as low capital costs. However, the main drawback of the SOE is that it suffers from safety issues and mechanically unstable electrodes in that they are prone to crack [7]. Alkaline media, on the other hand is mostly preferred for large commercial production compared to the other water electrolysis methods as it is a well-established method and uses cheaper materials (the use of non-noble electrodes such as nickel), and it is also relatively stable [7, 20, 29, 38, 43-45]. However, some of its drawbacks are slow dynamics

caused by the reactions occurring at the anode, gas permeations and corrosive electrolyte towards the electrode catalysts. In AWEs, the use of strongly alkaline aqueous solution as electrolyte such as potassium hydroxide and sodium hydroxide are employed to avoid corrosion caused by acidic electrolytes [7, 20]. The hydroxide ion (OH^-) acts as the charge carriers, preferably concentrated KOH (25-30 wt%) solution improves ionic conductivity over NaOH [30].

$$2H_2O \rightarrow O_2 + 2H_2 \qquad (E^\circ = -1.23\ V\ vs.\ SHE) \tag{7}$$

The general reaction for water electrolysis (7), is a nonspontaneous reaction (because of the negative cell potential) that readily, but not uniquely, needs energy that is provided by the flow of an electric current through an electrochemical cell [41, 46]. This equation sums up the hydrogen evolution (HER) at the cathode and oxygen evolution reaction (OER) at the anode that occur in water electrolysis as shown in Table 1.1. At 25 °C and 1 atm, the reactions and their standard equilibrium electrode potentials (E°) are described as follows:

Table 2.1: HER and OER involved in water electrolysis [15]

In alkaline medium		**E° (V) vs SHE**
Cathode	$4H_2O + 4e^- \rightarrow 2H_2 + 4OH^-$	-0.83
Anode	$4OH^- \rightarrow O_2 + 2H_2O + 4e^-$	0.40
In acidic medium		
Cathode	$4H^+ + 4e^- \rightarrow 2H_2$	0.0
Anode	$2H_2O \rightarrow O_2 + 4H^+ + 4e^-$	1.23

The theoretical decomposition voltage of water electrolysis, as per table 1.1 (standard electrode potentials listed as standard reduction potentials) at 25 °C and 1 atm is 1.23 V, which is the required voltage to generate hydrogen (under standard conditions) at a specific rate. This is also the equilibrium potential V_{eq} when considering the fundamental operating requirement of water splitting. The operational voltage V_{op} for water electrolysis system is dependent on the kinetics of water splitting and the design of the electrolyser unit such that:

$$V_{op} = V_{eq} + \eta_A + |\eta_C| + \eta_\Omega \tag{8}$$

In equation 8, η_A is the overpotential needed to overcome the kinetic barrier at the anode for the OER, and η_C is the overpotential required to overcome the kinetic barrier at the cathode for the HER. The resistance of the cell is compensated by the additional overpotential η_Ω within the device [41]. Based on equation 8 it can be concluded that the efficiency of an electrolyser system is determined from the deviation of V_{op} from V_{eq} [41]. It has been reported that the total overpotential (η) of a water electrolysis system in a 10% efficient integrated solar water-splitting system should be less than 0.45 V [36, 47, 48]. Consequently, it was proposed that a practical HER electrocatalyst should operate at a specific current density (j_s) of 10 mA.cm^{-2} at $\eta \sim 0.1$ V and an OER electrocatalyst should operate at j_s = 10 mA.cm^{-2} at $\eta \sim 0.35$ V [49, 50].

2.2 Oxygen evolution reaction (OER)

2.2.1 Background

The OER is one of the most important reactions in water electrolysis as it is the bottleneck reaction of the process. It has however, been studied to a much lesser extent compared to the HER due to its complexity and surface instability at common reaction potentials [25]. The OER is the limiting reaction in water electrolysis, which is evident from the high overpotentials that are required at the anode as a result of the sluggish kinetics of the OER [41, 43, 51, 52]. In AWE and PEM electrolysers, this is the main reason for energy losses during the electrolytic production of hydrogen [7, 53]. It is therefore imperative to reduce the energy losses and associated material costs through the development of effective and optimised oxygen evolution electrocatalysts [54].

As illustrated in Figure 2.1 the anode is the positive (+) electrode where the OER occurs for all electrolysis types. For AWE and PEM electrolysis reactions 9 and 10 are the OERs respectively [7, 41].

$$4OH^- \rightarrow O_2 + 2H_2O + 4e^- \qquad -0.83V \qquad (9)$$

$$2H_2O \rightarrow O_2 + 4H^+ + 4e^- \qquad 1.23V \qquad (10)$$

2.2.2 Mechanism of the OER and role of electrode surface

There is not a single mechanism/theory for the OER and a number of theories on the mechanism of the OER are presented in literature. This is because the mechanism of OER is far more complex, compared to the HER mechanism, and involves many intermediates such

as MO and, MOOH (M = metal). One famous mechanism path, for the alkaline OER (also known as Krasil'shchikov's path is described as follows:

$$M + OH^- \rightleftharpoons MOH + e^- \quad (11)$$

$$MOH + OH^- \rightleftharpoons MO^- + H_2O \quad (12)$$

$$MO^- \rightarrow MO + e^- \quad (13)$$

$$MO + MO \rightarrow 2M + O_2 \quad (14)$$

One of the charge transfers steps (Eqs. 11 and 12) is the rate controlling reaction. On a Ni electrode for example, at low temperature, the reaction is determined by a slow electron transfer. At high temperature, a slow recombination step (Eq. 14) controls the reaction [26, 38, 55].

2.2.3 Electrocatalysts for OER

Electrochemical water splitting suffers from substantial energy loss, mainly due to the high overpotential caused by the sluggish kinetics at the OER. To this regard, optimal oxygen-evolving electrocatalysts have been sought after to minimise this energy loss [56]. Research has identified IrO_2 and RuO_2, alone or in combination as the reference OER catalysts both in acid and alkaline conditions [46, 57, 58]. However, their scarcity and high costs have been the driving force behind the extensive search for the development of alternative low-cost, durable and highly active catalysts [7]. IrO_2 and RuO_2 also have a shortcoming of not being "ideal" catalysts for OER, this has been proven through thermodynamic calculations that suggest that RuO_2 binds oxygen too quickly, consequently obstructing the oxidation of HO^*. On the other end IrO_2 binds oxygen a little too strongly, which in turn hinders the formation of HOO^* [46]. The specific current density (j_s) in 0.1 M KOH of the OER has recently been investigated for laser deposited films of Ir and Ru on (001)-oriented $SrTiO_3$ and it was reported that j_s is ~ 0.4 $mA.cm^{-2}$ and ~ 0.03 $mA.cm^{-2}$ at η= 0.35V for the RuO_2(110) and Ir(100) respectively [59].

It is desirable that an electrocatalyst should exhibit very low overpotential for the anodic OER, be of low cost and have long term stability against corrosion. Platinum has also been investigated in search for a less expensive metal as electrocatalyst for water electrolysis as it has proven to be the best cathodic electrocatalyst for the oxygen reduction reaction (ORR) in fuel cells, by exhibiting high current densities at negligible overpotentials [60]. However, Pt shows moderate activity towards the oxygen evolution reaction (OER). This has led to the

development of Pt-based bifunctional alkaline water electrolysis catalysts [61]. To this regard, research shows that the addition of Pt to oxides such as Pt-$CaMnO_3$ and Pt-TiO_2 has shown improvement in anode activity, stability and conductivity in alkaline electrolysis [54, 62, 63]. Pt-$CaMnO_3$, which was obtained by the intermittent microwave heating and chemical reduction method exhibited an overpotential of 95 mV and a high current density of 5.2 $mA.cm^{-2}$. These remarkable observations were attributed to the synergistic effect of Pt, Mn_3O_4 and C that enabled the composites to enhance the surface area as well as the conductivity for charge transport for the OER [61]. Nonetheless, the lack in abundance of Pt and its associated high cost remain its biggest drawback [61].

Considering the cost and scarcity of noble metals such as ruthenium (Ru), iridium (Ir) and platinum (Pt), non-noble metals such as nickel has been considered as the material of choice when developing electrodes for alkaline water electrolysis [7]. This is due to the fact that nickel exhibits good activity and stability in alkaline media [17, 61, 64]. Although, cobalt and nickel oxides, electrocatalysts, for example are not stable under OER conditions in acidic medium, due to their thermodynamic instability under oxidative conditions and their quite large associated overpotentials [56], in alkaline medium most electrocatalysts are stable and achieve 10 $mA.cm^{-2}$ current densities at $\eta = 0.35 \sim 0.50$ V for OER [49, 50, 65]. Conventionally, the preferred anode material for alkaline water electrolysis systems has been made from nickel or nickel-coated steel. However, in 1961 highly porous Raney nickel (a combination of nickel and aluminium) was discovered as an effective material for cathodes in the production of electrolytic hydrogen [66, 67]. During the production process of Raney nickel powder, the material is activated by the aluminium leaching from the Ni-Al alloy, the leaching process results in the formation of lattice vacancies, which result in large surface areas and a high density of active sites due to high density of reactive lattice defects. The activated electrocatalyst therefore provides better performance compared to un-activated nonporous nickel [17]. Plasma spraying preparation of a Raney nickel composite was also conducted by Kjartansdottir and co-workers employing Ni-Al powder and Co_3O_4 particles [17, 28, 67]. The electrocatalyst obtained exhibited a reduction in the OER overpotential of ~150 mV when compared to elemental nickel, with stability being acceptable [17, 67]. Studies have shown that independent of the procedure for its preparation; Raney nickel has proven to be superior to pure nickel [17, 67]. Raney nickel has furthermore been reported to be a better anode electrocatalyst when compared to other active electrocatalysts such as $NiCo_2O_4$, Co_3O_4 and $LaNiO_3$ [45]. It can be added that modifications of Ni and nickel-oxide based materials through alloying and doping may result in higher activity for the hydrogen and oxygen evolution reactions [60]. Additionally, Ni-Fe, Ni-Co, Ni-Bi and Ni-Zn electrocatalysts have also been identified as promising alternatives compared to that of noble metals such Pt, Ru and Pd,

which is due to the synergistic characteristics of the elements forming the alloy as well as the increased surface area obtained [30, 68]. Another advantage of employing Ni-based alloys, by combining Ni with other transition metals such as Pt, is the high adsorption ability of Ni atoms [30].

Unlike nickel and platinum, no research has been done on employing pure aluminium as an electrocatalyst for the OER in alkaline medium. Aluminium is a poor electrocatalyst on its own, and has only been used in Raney Nickel due to it leaching and thereby activating the electrocatalyst [67].

2.2.4 Electrocatalyst development

Various techniques can be employed experimentally to investigate and determine the activity and stability, as well as other properties, of electrocatalyst materials incorporated on electrolyser electrodes. Electrodes are defined as either bulk or thin film (substrate supported) electrodes. A bulk electrode (e.g. a polycrystalline Pt disc) only consists of the electrocatalyst material itself, whereas a thin film (e.g. Pt nanoparticles on a carbon support) consists of the electrocatalyst material deposited onto an inert support material (e.g. Vulcan carbon or glassy carbon insert).

Bulk electrodes are mostly used in the study of pure material electrocatalysts. These electrodes are usually purchased from third party suppliers as only a few research entities have the right equipment to produce these electrode inserts, especially when novel materials i.e. bi, tri-metallic electrocatalysts are employed. However, these bulk electrodes are still being employed in electrochemical research due to their substantial low material cost and possible increase in performance offered by these electrode designs [69].

On the other hand, thin film electrodes (which can be referred to as electrodes incorporating a few nanometres, micrometres or more of catalyst) with an inert support material that does not interfere with the flow of current are comparable to bulk electrodes because electron transfer only occurs at the electrode-electrolyte interface [70]. The most widely employed support material for thin film electrodes is carbon, due to its large specific surface area, excellent chemical stability and conductivity [69, 71]. In this study, we make use of glassy carbon (GC) inserts as support material due to their wide range of chemical and physical property advantages such as hardness, low permeability to liquids and gases as well as being able to operate within a wide potential range [72, 73]. Various physical (physical vapour deposition) and chemical (chemical vapour deposition, electroplating) techniques are available for the deposition of catalysts on supports such as GC's. Physical vapour deposition

techniques consist of various methods that are widely used to ensure deposition of any catalyst materials on a wide variety of supports. These methods include electron beam deposition, pulsed laser deposition and sputter deposition (which will be used in this study, specifically combinatorial sputtering) [74, 75]. Combinatorial sputtering allows for effective rapid and uniform deposition of metal particles over a large area [75].

2.3 Combinatorial and high-throughput methods

Research in the 21st century has benefitted a lot from technological advances related to the research, development and optimisation of materials having improved properties. Through these technological advances, materials have been developed that offer enhanced performance, reduced cost and increased environmental friendliness. In 1970, Hanak made one of the first remarks with regards to multi-sample development and testing, stating that present approaches that test one sample at a time are tedious, expensive and time-consuming that prevents researchers from working effectively towards the discovery of new materials [76]. He suggested that processing of many different materials at the same time will significantly increase the productivity of material research. A number of studies have highlighted the benefits of high-throughput and combinatorial (HTC) methodologies that can be applied as means of parallel synthesis, property characterisation and the rapid development of novel functional materials [77-79]. Combinatorial and high-throughput experimentation is a process that is recognised especially in the discovery and optimization of new material with the advantage of avoiding time-consuming synthesis and testing of numerous materials that are brought about by the complexity exhibited by the structural and functional properties of the materials [80]. Material composition is not the only property that new material development depends on in material science, but also on morphology, microstructure and preparation, just to name a few. This complexity has resulted in the recognition of HTC technologies/methods as a new scientific approach for the fabrication and simultaneous characterisation of a great number of materials under the same conditions. Historically, combinatorial methodologies were mostly applicable to the pharmaceutical, biological and medical disciplines [77], however, recent years have witnessed the discovery and optimization of homogeneous and heterogeneous catalysts, and new materials, through these combinatorial and high-throughput approaches. With regards to heterogeneous catalysis, combinatorial library synthesis can be carried out by a variety of solution and vapour deposition methods with the catalytically active sites existing on the interior and/or exterior surface of the solid-state inorganic material. This technique can be used to explore new materials that consist of up to three, four or more compositional elements having different physical and chemical properties [79, 80]. It goes without saying that there is a wide range of possible catalyst variations due to the number of

elements on the periodic table [80]. Moreover, for solid heterogeneous materials it becomes more complex for complete specification to be done due to the number of properties required for solid state characterisation such as crystallinity, interphase properties, surface and bulk property differences, etc. which increase the series of possibilities on a systematic basis [80]. In order to assist heterogeneous catalyst design, computational chemistry and applying known knowledge about the system being catalysed are two ways in which the number of possible catalysts to be tested have been reduced [80, 81]. However, in comparison to conventional linear and sequential methodologies that provide a high chance of accurate experimentation, HTC does not always allow for highly accurate and precise experimentation [82, 83]. It is rather aimed at probing observable trends related to the material of interest e.g. catalytic activity, subsequent to initial observations previously obtained by means of traditional methods [84, 85].

Although HTC is still a new paradigm for many researchers, it has been found very attractive for the combinatorial synthesis and high-throughput screening of inorganic electrocatalytic materials [77, 78, 86]. This is because electrochemical methods have several screening variables under direct control such as voltage, current and electrolyte whether manual or by automated programming [78].

2.4 Electrocatalysts characterisation

2.4.1 Three-electrode electrochemical cell

After the deposition/sputtering of the electrocatalysts on the GC electrode inserts, they can be characterised in an electrochemical cell coupled to a potentiostat (Figure 2.2). A standard three-electrode cell (Figure 2.2) setup consists of a counter electrode (CE), a working electrode (WE), and a reference electrode (RE). By means of a potentiostat (the heart of electrochemistry), a potential is applied to the working electrode where the reaction of interest occurs on the electrode surface (at the electrode electrolyte interface). The change in potential of the WE is measured against the RE (with a known fixed potential). The type of WE employed in this research project is a rotating disk electrode (RDE). This setup allows for change in (i) the applied potential (E.mV), (ii) the potential scan rate (v, $mV.s^{-1}$) and (iii) the electrode rotation rate (ω, rpm). By employing a RDE, the mass transport of the active species, from the bulk of the electrolyte to the electrode surface can be increased due to increased convection, i.e. the higher the rate of rotation, the higher rate of transport to the surface of the electrode. As a result of the electrochemical reaction occurring at the surface of the WE, a current is generated due to the electron transfer between the active species and the electrode surface,

with the amount of current flowing being monitored by the CE (electrons flowing in the electrical circuit and ionic species flowing in the electrolyte between the WE and CE). It is on the surface of the WE where the oxidation reaction (OER) actually takes place, which is preceded by adsorption of the active species onto the electrode surface following transport of the active species from the electrolyte solution (0.1 M KOH in alkaline medium) to the surface of the WE. This adsorption of strong species will enable electron transfer [87].

Employing this setup, linear sweep voltammetry (LSV) measurements will be conducted to compare the activity of different electrocatalysts in this research project.

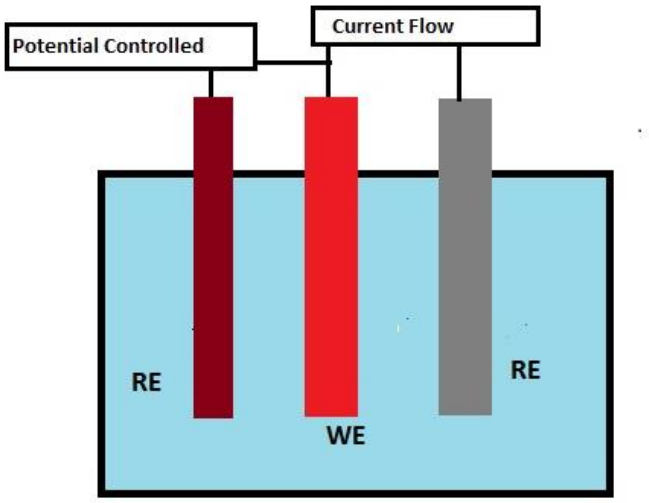

Figure 2.2. A standard three-electrode cell setup

2.4.2 Linear sweep voltammetry

Linear sweep voltammetry (LSV) is the key electrochemical technique employed as part of this investigation to determine the catalysts' activity towards the OER in alkaline medium. In this technique, the current is measured as a function of potential (which is varied between two potential values, E_{low} and E_{high}). For the OER, an oxidation/anodic reaction, the LSV (Figure 2.3) is a typical example, with the potential scan being performed in the positive potential direction producing a positive oxidation/anodic current.

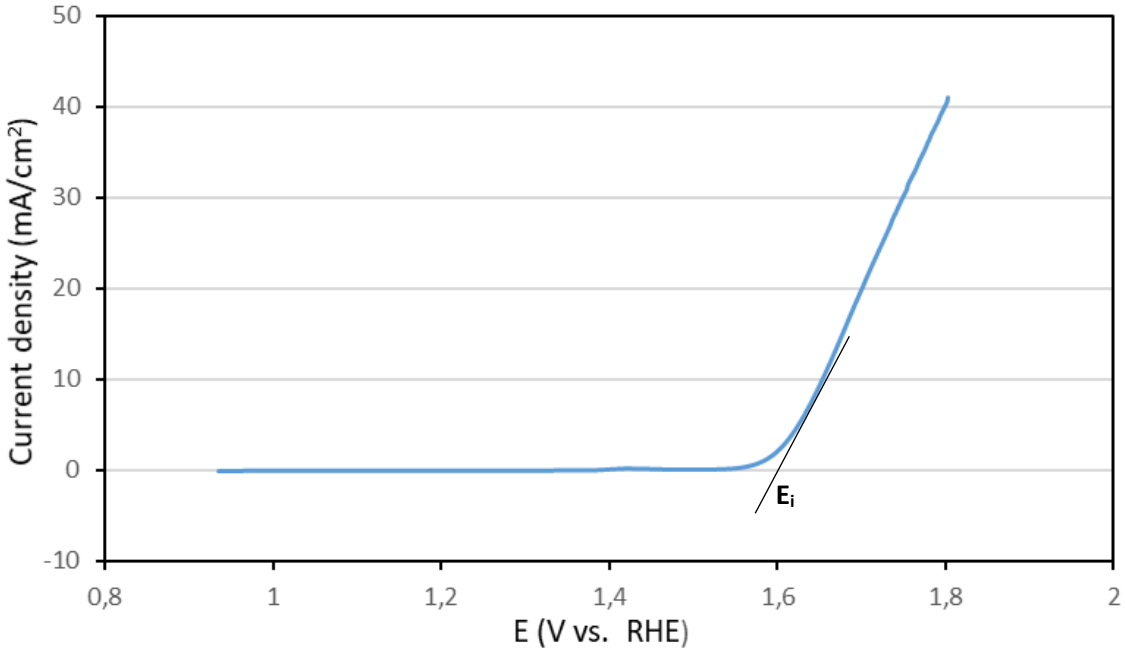

Figure 2.3. Typical linear sweep voltammetry (LSV) curve for an anodic reaction (E_i is the onset potential)

At the equilibrium potential no current is flowing as neither oxidation nor reduction occurs, and the current (or current density) is zero. A potential greater than the equilibrium potential, i.e. an overpotential (η), needs to be applied for the reaction to occur. Very close to the equilibrium potential, the current density is initially zero, electron transfer occurs because the surface concentration of the reactant is still very high. At this point, the current density is strongly dependent on the potential and does not vary with the electrode rotation rate, and this region is therefore governed by kinetic control. As the potential is increased (at intermediate potentials), the surface concentrations of the electroactive species become less than that of the bulk due to oxidation/reduction taking place, but has not reached zero yet.

The comparison of the activities of the catalysts will be done based on information on the onset potentials (E_i, Figure 2.3) and current densities ($mA.cm^{-2}$). The potential at which the reaction starts is known as the onset potential of the catalyst on a LSV scan. A good catalyst is therefore one that has a low onset potential (for anodic oxidation reaction), as well as a higher peak current density. For the catalyst to be effective for the reaction, it is important that the reaction proceeds at a reversible or equilibrium potential. Problems such as a high overpotential often arise when the applied potential required to drive the reaction deviates extremely from the reaction's standard electrode equilibrium potential [87].

2.4.3 Chronopotentiometry

Chronopotentiometry (CP), a controlled current technique, is a voltammetry technique that is used to study electrochemical behaviour, especially electrocatalyst stability/durability. During CP a controlled and constant current is applied between the working and counter electrodes such that the resulting potential of the working electrode is measured against the reference electrode. This technique is used to test the stability of electrocatalysts over prolonged time periods.

2.4.4 Tafel slope

Electrochemical reaction kinetics can be scrutinised using the Tafel slope, with a large Tafel slope indicating a kinetically sluggish reaction and smaller Tafel slope indicating a reaction with favourable kinetics [70].

The Tafel equation of the OER can be expressed in the following form:

$$j = j_a = j_0 \exp \frac{\alpha_a . nF\eta}{RT} \quad (15)$$

Equation (15) represents the relationship between the steady-state anodic current and the applied overpotential, where j is the experimental current density (mA.cm^{-2}), j_a is the anodic current density (mA.cm^{-2}), j_0 is the exchange current density (mA.cm^{-2}), α is the transfer coefficient, n is the number of electrons involved in the electrode reaction, F is Faraday's constant (C.mol^{-1}), η is the overpotential (V), R is the universal gas constant and T the temperature (K).

To determine the transfer coefficient α, the Tafel equation can be written in the following form for anodic reactions (equation 16) and cathodic reactions (equation 17) [88]:

$$\log j = \log j_0 + \frac{\alpha_a . nF\eta}{2.3RT} \quad (16)$$

$$\log (-j) = \log j_0 - \frac{\alpha_c . nF\eta}{2.3RT} \quad (17)$$

Where the subscripts 'a' and 'c' for the transfer coefficient (α) refer to the anodic and cathodic form of the current potential relationship. However, in this study, only the anodic OER current will be of interest, which can be expressed in logarithmic form as follows:

$log\ j = \log j_0 + \frac{\eta}{b}$ (18)

Equation (18) can be written in the initial form as proposed by Tafel in 1904 [87] as:

$$\eta = a + blog\ (i) \quad (19)$$

Equation (19) shows that current is exponentially related to overpotential, where *α* is a constant and *b* is the Tafel slope given by:

$$log\ j = \frac{\partial \eta}{\partial log i} = \frac{2.303RT}{\alpha.F} \quad (20)$$

The Tafel slope b ($mV.dec^{-1}$) can be extracted from the slope of the plots of log(j) vs. η or η vs. log(j) [87].

References

1. M. Ball, M. Wietschel, *The future of hydrogen – opportunities and challenges.* International Journal of Hydrogen Energy, 2009. **34**(2): p. 615-627.
2. J. Chamie, *World population : 2020 overview.* 2020.
3. Agency, I.E. *Global Energy and CO_2 report*. [cited 2019 2019/09/06]; Available from: https://www.iea.org/geco/.
4. *International energy agency, World energy outlook 2014 Executive summary*. [cited 2019 2019/09/06]; Available from: http://www.iea.org/textbase/npsum/weo2014sum.pdf.
5. C.A. Miller, *Energy Resources and Policy.* 2013: p. 37-51.
6. J. Speirs, C. McGlade, R. Slade, *Uncertainty in the availability of natural resources: Fossil fuels, critical metals and biomass.* Energy Policy, 2015. **87**: p. 654-664.
7. F.M. Sapountzi, J.M. Gracia, C.J. Weststrate, H-O.A. Fredriksson, J.W. Niemantsverdriet, *Electrocatalysts for the generation of hydrogen, oxygen and synthesis gas.* Progress in Energy and Combustion Science, 2017. **58**: p. 1-35.
8. M. Asif, T. Muneer, *Energy supply, its demand and security issues for developed and emerging economies.* Renewable and Sustainable Energy Reviews, 2007. **11**(7): p. 1388-1413.
9. M. Saxe, P. Alvfors, *Advantages of integration with industry for electrolytic hydrogen production.* Energy, 2007. **32**(1): p. 42-50.
10. H.Z. Wang, D.Y.C. Leung, M.K.H. Leung, M. Ni, *A review on hydrogen production using aluminum and aluminum alloys.* Renewable and Sustainable Energy Reviews, 2009. **13**(4): p. 845-853.
11. J.L. Steimke, T.J. Steeper, H.R. Colon-Mercado, *Development and testing of a PEM SO_2-depolarized electrolyzer and an operating method that prevents sulfur accumulation.* International Journal of Hydrogen Energy, 2015. **40**(39): p. 13281-13294.
12. R.A. Hefner III, *The age of gases.* International Journal of Hydrogen Energy, 2002. **27**: p. 1-9.
13. C.J. Winter, *Hydrogen energy — Abundant, efficient, clean: A debate over the energy-system-of-change☆.* International Journal of Hydrogen Energy, 2009. **34**(14): p. S1-S52.
14. K. Kovacs, G. Maroti, G. Rakhely, *A novel approach for biohydrogen production.* International Journal of Hydrogen Energy, 2006. **31**(11): p. 1460-1468.

15. M. Wang, Z. Wang, X. Gong, Z. Guo, *The intensification technologies to water electrolysis for hydrogen production – A review.* Renewable and Sustainable Energy Reviews, 2014. **29**: p. 573-588.
16. D.L. Stojić, M.P. Marceta, S.P. Sovilj, S.S. Miljanic, *Hydrogen generation from water electrolysis—possibilities of energy saving.* Journal of Power Sources, 2003. **118**(1-2): p. 315-319.
17. C.K. Kjartansdóttir, L.P. Nielsen, P. Møller, *Development of durable and efficient electrodes for large-scale alkaline water electrolysis.* International Journal of Hydrogen Energy, 2013. **38**(20): p. 8221-8231.
18. L. Barelli, G. Bidini, F. Gallorini, S. Servili., *Hydrogen production through sorption-enhanced steam methane reforming and membrane technology: A review.* Energy, 2008. **33**(4): p. 554-570.
19. A. Simpson, A. Lutz, *Exergy analysis of hydrogen production via steam methane reforming.* International Journal of Hydrogen Energy, 2007. **32**(18): p. 4811-4820.
20. D.M. Santos, A.C. Sequeira, J.L. Figueiredo , *Hydrogen production by alkaline water electrolysis.* Quimica Nova, 2013. **36**(8): p. 1176-1193.
21. M.A. Oliver-Tolentino, J. Vazquez-Samperio, A. Manzo-Robledo, R. Gonzalez-Huerta, J.L. Flores-Moreno, D. Ramirez-Rosales, A. Guzman-Vargas, *An Approach to Understanding the Electrocatalytic Activity Enhancement by Superexchange Interaction toward OER in Alkaline Media of Ni–Fe LDH.* The Journal of Physical Chemistry C, 2014. **118**(39): p. 22432-22438.
22. S. Marini, P. Salvi, P. Nelli, R. Pesenti, M. Villa, Y. Kiros, *Oxygen evolution in alkali with gas diffusion electrodes.* International Journal of Hydrogen Energy, 2013. **38**(26): p. 11496-11506.
23. A. Falch, V. Lates, R.J. Kriek, *Combinatorial Plasma Sputtering of PtxPdy Thin Film Electrocatalysts for Aqueous SO2 Electro-oxidation.* Electrocatalysis, 2015. **6**(3): p. 322-330.
24. R.G. González-Huerta, G. Ramos-Sánchez, P.B. Balbuena, *Oxygen evolution in Co-doped RuO_2 and IrO_2: Experimental and theoretical insights to diminish electrolysis overpotential.* Journal of Power Sources, 2014. **268**: p. 69-76.
25. S. Cherevko, S. Geiger, O. Kasian, N. Kulyk, J-P. Grote, A. Savan, B.R. Shrestha, S. Merzlikin, B. Breitbach, A. Ludwig and K.J.J Mayrhofer *Oxygen and hydrogen evolution reactions on Ru, RuO_2 , Ir, and IrO_2 thin film electrodes in acidic and alkaline electrolytes: A comparative study on activity and stability.* Catalysis Today, 2016. **262**: p. 170-180.

26. M.Z. Iqbal, R.J. Kriek, *Silver/Nickel Oxide (Ag/NiO) Nanocomposites Produced Via a Citrate Sol-Gel Route as Electrocatalyst for the Oxygen Evolution Reaction (OER) in Alkaline Medium.* Electrocatalysis, 2018. **9**(3): p. 279-286.
27. J.L. Corona-Guinto, L. Cardeno-Garcia,D.C. Martinez-Casillas, J.M. Sandoval-Pineda, P. Tamayo-Meza, R. Silva-Casarin, R.G. Gonzalez-Huerta, *Performance of a PEM electrolyzer using RuIrCoOx electrocatalysts for the oxygen evolution electrode.* International Journal of Hydrogen Energy, 2013. **38**(28): p. 12667-12673.
28. V. Maruthapandian, T. Pandiarajan, V. Saraswathy, S. Muralidharan, *Oxygen evolution catalytic behaviour of Ni doped Mn_3O_4 in alkaline medium.* RSC Advances, 2016. **6**(54): p. 48995-49002.
29. X. Li, F.C. Walsh, D. Pletcher, *Nickel based electrocatalysts for oxygen evolution in high current density, alkaline water electrolysers.* Phys Chem Chem Phys, 2011. **13**(3): p. 1162-7.
30. S. Seetharaman, R. Balaji, K. Ramya, K.S. Dhathathreyan, M. Velan, *Electrochemical behaviour of nickel-based electrodes for oxygen evolution reaction in alkaline water electrolysis.* Ionics, 2013. **20**(5): p. 713-720.
31. M. Momirlan, T. Veziroglu, *The properties of hydrogen as fuel tomorrow in sustainable energy system for a cleaner planet.* International Journal of Hydrogen Energy, 2005. **30**(7): p. 795-802.
32. A. Caillard, C. Coutanceau, P. Brault, J. Mathias, J.M. Leger, *Structure of Pt/C and PtRu/C catalytic layers prepared by plasma sputtering and electric performance in direct methanol fuel cells (DMFC).* Journal of Power Sources, 2006. **162**(1): p. 66-73.
33. T. Reier, M. Oezaslan, P. Strasser, *Electrocatalytic Oxygen Evolution Reaction (OER) on Ru, Ir, and Pt Catalysts: A Comparative Study of Nanoparticles and Bulk Materials.* ACS Catalysis, 2012. **2**(8): p. 1765-1772.
34. M.H. Miles, E.A. Klaus, B.P. Gunn, J.R. Locker, W.E. Serafin, *The oxygen evolution reaction on platinum, Iridium, Ruthenium and their alloys at 80°C in acidic solutions*. Electrochemica Acta, 1978 23:p. 521-526
35. M.D. Mamoon Rahid, M.K. Al Mesfer, H. Naseem, M. Danish, *Hydrogen Production by Water Electrolysis A review of alkaline water electrolysis, PEM, and high temperature water electrolysis.* Internationl Journal of Engineering and Advanced Technology, 2015. **4**(3): p. 80-93.
36. M.F. Weber, M. Dignam, *Splitting water with semiconducting photoelectrodes—Efficiency considerations.* International Journal of Hydrogen Energy, 1986. **11**(4): p. 225-232.

37. E. Mayousse, F. Maillard, F. Fouda-Onana, O. Sicardy, N. Guillet, *Synthesis and characterization of electrocatalysts for the oxygen evolution in PEM water electrolysis.* International Journal of Hydrogen Energy, 2011. **36**(17): p. 10474-10481.
38. K. Zeng, D. Zhang, *Recent progress in alkaline water electrolysis for hydrogen production and applications.* Progress in Energy and Combustion Science, 2010. **36**(3): p. 307-326.
39. J.C. Ganley, *High temperature and pressure alkaline electrolysis.* International Journal of Hydrogen Energy, 2009. **34**(9): p. 3604-3611.
40. F. Barbir, *PEM electrolysis for production of hydrogen from renewable energy sources.* Solar Energy, 2005. **78**(5): p. 661-669.
41. R.L. Doyle, M.E.G. Lyons, *The Oxygen Evolution Reaction: Mechanistic Concepts and Catalyst Design.* 2016: p. 41-104.
42. G. Lu, J.S. Cooper, P.J. McGinn, *SECM characterization of Pt–Ru–WC and Pt–Ru–Co ternary thin film combinatorial libraries as anode electrocatalysts for PEMFC.* Journal of Power Sources, 2006. **161**(1): p. 106-114.
43. J. Kubisztal, A. Budniok, *Study of the oxygen evolution reaction on nickel-based composite coatings in alkaline media.* International Journal of Hydrogen Energy, 2008. **33**(17): p. 4488-4494.
44. C. Tang, N. Cheng, Z. pu, W. Xing, X. Sun, *NiSe Nanowire Film Supported on Nickel Foam: An Efficient and Stable 3D Bifunctional Electrode for Full Water Splitting.* Angew Chem Int Ed Engl, 2015. **54**(32): p. 9351-5.
45. J. Divisek, P. Malinowski, J. Mergel, H. Schmitz, *Improved components for advanced alkaline water electrolysis.* International journal of hydrogen energy, 1988. **13**(3): p. 141-150.
46. S. Marini, P. Salvi, P. Nelli, R. Pesenti, M. Villa, M. Berrettoni, G. Zangari, Y. Kiros, *Advanced alkaline water electrolysis.* Electrochimica Acta, 2012. **82**: p. 384-391.
47. M.G. Walter, E.L. Warren, J.R. McKone, S.W. Boettcher, Q. Mi, E.A. Santori, N.S. Lewis, *Solar water splitting cells.* Chemical reviews, 2010. **110**(11): p. 6446-6473.
48. M.F. Weber, M.J. Dignam, *Efficiency of splitting water with semiconducting photoelectrodes.* Journal of The Electrochemical Society, 1984. **131**(6): p. 1258-1265.
49. C.C. McCrory,S. Jung, J.C. Peters, T.F. Jaramillo, *Benchmarking heterogeneous electrocatalysts for the oxygen evolution reaction.* J Am Chem Soc, 2013. **135**(45): p. 16977-87.
50. C.C. McCrory, S. Jung, I.M. Chatman, J.C. Peters, T.F. Jaramillo, *Benchmarking hydrogen evolving reaction and oxygen evolving reaction electrocatalysts for solar water splitting devices.* J Am Chem Soc, 2015. **137**(13): p. 4347-57.

51. M.S. Burke, L.J. Enman, A.S. Batchellor, S. Zou, S.W. Boettcher, *Oxygen Evolution Reaction Electrocatalysis on Transition Metal Oxides and (Oxy)hydroxides: Activity Trends and Design Principles.* Chemistry of Materials, 2015. **27**(22): p. 7549-7558.
52. H. Osgood, S.V. Devaguptapu, H. Xu, G. Wu, *Transition metal (Fe, Co, Ni, and Mn) oxides for oxygen reduction and evolution bifunctional catalysts in alkaline media.* Nano Today, 2016. **11**(5): p. 601-625.
53. Y. Cheng, *Advances in electrocatalysts for oxygen evolution reaction of water electrolysis-from metal oxides to carbon nanotubes.* Progress in natural science: materials international, 2015. **25**(6): p. 545-553.
54. C. Xu, L. Ma, J. Li, W. Zhao, Z. Gan, *Synthesis and characterization of novel high-performance composite electrocatalysts for the oxygen evolution in solid polymer electrolyte (SPE) water electrolysis.* International Journal of Hydrogen Energy, 2012. **37**(4): p. 2985-2992.
55. G. Li, L. Anderson, Y. Chen, M. Pan, P. Abel-Chuang, *New insights into evaluating catalyst activity and stability for oxygen evolution reactions in alkaline media.* Sustainable Energy & Fuels, 2018. **2**(1): p. 237-251.
56. M.García-Mota, A. Vojvodic, H. Metiu, I.C. Man, H-Y. Su, J. Rossmeisl, J.K. Norskov, *Tailoring the Activity for Oxygen Evolution Electrocatalysis on Rutile TiO_2(110) by Transition-Metal Substitution.* ChemCatChem, 2011. **3**(10): p. 1607-1611.
57. Y. Lee, J.Suntivich, K.J. May, E.E. Perry, Y. Shao Horn, *Synthesis and activities of rutile IrO_2 and RuO_2 Nanoparticles for oxygen evolution in acid and alkaline solutions.* Journal of physical chemistry letters, 2012. **3**(3): p. 399-404.
58. A. Minguzzi, F.-R.F.Fan, A. Vertova, S. Rondinini, A.J. Bard, *Dynamic potential-pH digrams application to electrocatalysts for water oxidation.* Chemical science, 2012. **3**: p. 217-229.
59. K.A. Stoerzinger, L. Qiao, M.D. Biegalski, Y. Shao-Horn, *Orientation-dependent oxygen evolution activities of rutile IrO_2 and RuO_2.* The journal of physical chemistry letters, 2014. **5**(10): p. 1636-1641.
60. L. Elias, K. Scott, A.C. Hegde, *Electrolytic Synthesis and Characterization of Electrocatalytic Ni-W Alloy.* Journal of Materials Engineering and Performance, 2015. **24**(11): p. 4182-4191.
61. Z.Y. Li, S.T. Shi, Q.S. Zhong, C.J. Zhang, C-W. Xu, *Pt-Mn_3O_4/C as efficient electrocatalyst for oxygen evolution reaction in water electrolysis.* Electrochimica Acta, 2014. **146**: p. 119-124.
62. S.H. Ahn, I. Choi, H.Y. Park, S.J. Hwang, S.J. Yoo, E. Cho, H.J. Kim, D. Henkensmeier, S.W. Nam, S.K. Kim, J.h. Jang, *Effect of morphology of electrodeposited Ni catalysts*

on the behavior of bubbles generated during the oxygen evolution reaction in alkaline water electrolysis. Chem Commun (Camb), 2013. **49**(81): p. 9323-5.

63. I.M. Sadiek , M.A., El-Shakre ME, Awad MI, El-Deab MS, Anadouli BE, *Electrocatalytic Evolution of Oxygen Gas at Cobalt Oxide Nanoparticles Modified Electrodes.* International Journal of electrochemical science, 2012. **7**(4): p. 3350-3361.
64. M. Vanags, J. Kleperis, G. Bajars, A. Lusis, *Water electrolysis using electrodes with modified surface/volume.* Journal of Physics: Conference Series, 2007. **93**: p. 012025.
65. S. Jung, C.C.L. McCrory, I.M. Ferrer, J.C.Peters, T.F. Jaramillo, *Benchmarking nanoparticulate metal oxide electrocatalysts for the alkaline water oxidation reaction.* Journal of Materials Chemistry A, 2016. **4**(8): p. 3068-3076.
66. Y. Choquette , H. Menard, L. Brossard, *Electrocatalytic performance of composite-coated electrodes for alkaline water electrolysis.* International Journal of Hydrogen Energy, 1990. **15**(1): p. 21-26.
67. C. Kjartansdóttir, M. Caspersen, S. Egelund, P. Moller , *Electrochemical investigation of surface area effects on PVD Al-Ni as electrocatalyst for alkaline water electrolysis.* Electrochimica Acta, 2014. **142**: p. 324-335.
68. M.W. Louie, A.T. Bell, *An investigation of thin-film Ni-Fe oxide catalysts for the electrochemical evolution of oxygen.* J Am Chem Soc, 2013. **135**(33): p. 12329-37.
69. S.A. Grigoriev, A.A. Fedotov, S.A. Matemianov, V.N. Fateev, *Synthesis of nanostructural electrocatalytic materials on various carbon substrates by ion plasma sputtering of platinum metals.* Russian Journal of Electrochemistry, 2014. **50**(7): p. 638-646.
70. A.J. Bard, L.R. Faulkner, *Fundamentals and applications.* Electrochemical Methods, 2001. **2**: p. 482.
71. O.K. Alexeeva, V.N. Fateev, *Application of the magnetron sputtering for nanostructured electrocatalysts synthesis.* International Journal of Hydrogen Energy, 2016. **41**(5): p. 3373-3386.
72. C. Quijada, J. Vazquez, *Electrochemical reactivity of aqueous SO2 on glassy carbon electrodes in acidic media.* Electrochimica acta, 2005. **50**(27): p. 5449-5457.
73. A. Dekanski, J. Stevanovic, R. Stevanovic, B.Z. Nikolic, V.M. Jovanovic *Glassy carbon electrodes: I. Characterization and electrochemical activation.* Carbon, 2001. **39**(8): p. 1195-1205.
74. O.K Alexeeva,V.N. Fateev , *Applictaion of the magnetron sputtering for nanostructured electrocatalysts synthesis.* International Journal of Hydrogen Energy, 2016. **41**: p. 3373-3386.

75. J-E. Lim, J.K.K. Jeong, K.H. Ahn, H.J. Kim, C.S. Hwang, D-Y. Park, D-S. Lee, *Microstructural characterization of sputter-deposited Pt thin film electrode.* Journal of materials science, 2004. **19**: p. 460-468.
76. J.J. Hanak, *The Multiple-Sample Concept in Material Research: synthesis, computational analysis and testing of entire multicomponent systems.* Journal of materials science, 1970. **5**: p. 964-971.
77. T.H. Muser, A. Trinchi, T.A. Markley, D. Lau, P. Martin, A. Bradbury, A. Bendavid, S. Dligath, *A review of high throughput and combinatorial electrochemistry.* Electrochimica Acta, 2011. **56**(27): p. 9679-9699.
78. S.H. Baeck, T.F. Jaramillo, A. Kleinman-Shwaesctein, E.W.McFarland, *Automated electrochemical synthesis and characterization of TiO_2supported Au nanoparticle electrocatalysts.* Measurement Science and Technology, 2005. **16**(1): p. 54-59.
79. B.Jandeleit, D.J. Schaefer, T.S. Powers, H.W. Turner, *Combinatorial Material Science.* Angewandte_Chemie_International_Edition, 1999. **38**: p. 2494-2532.
80. R. Potyrailo, K. Rajan, K. Stoewe, I. Takeuchi, B. Chisholm, H. Lam, *Combinatorial and high-throughput screening of materials libraries: review of state of the art.* ACS Comb Sci, 2011. **13**(6): p. 579-633.
81. S. Schunk, A. Sundermann, H. Hibst, *Structure oriented library design in gas phase oxidation catalysis.* Catalysis Today, 2008. **137**(1): p. 36-43.
82. J. Loskyll, K. Stoewe, W.F. Maier, *High-throughput technology for novel SO2 oxidation catalysts.* Sci Technol Adv Mater, 2011. **12**(5): p. 054101.
83. W.F. Maier, K. Stowe, S. Sieg, *Combinatorial and high-throughput materials science.* Angew Chem Int Ed Engl, 2007. **46**(32): p. 6016-67.
84. P, Strasser, Q. Fan, M. Devenney, W. H. Weinberg, *High Throughput Experimental and Theoretical Predictive Screening of Materials.* J. Phys. Chem., 2003. **107**: p. 11013-11021.
85. A.S. Bandarenka, E. Vemtosa, A. Maljusch, J. Masa, W. Schuhmann, *Techniques and methodologies in modern electrocatalysis: evaluation of activity, selectivity and stability of catalytic materials.* Analyst, 2014. **139**(6): p. 1274-91.
86. J.G. Hauck, P.J. McGinn, *Screening of Novel Li–Air Battery Catalyst Materials by a Thin Film Combinatorial Materials Approach.* ACS Combinatorial Science, 2015. **17**(6): p. 355-364.
87. D. Pletcher, *A first course in electrode processes*. 2019: Royal Society of Chemistry.
88. D. Pletcher, X. Li, *Prospects for Alkaline Zero Gap Electrolyte Water Electrolysers.* Elsevier, 2011. p. 1-45.

3 ARTICLE

Optimisation of $Pt_xNi_yAl_z$ ratios as thin film electrocatalysts for the oxygen evolution reaction (OER) in alkaline medium

HK Kishinkwa, A Falch, RJ Kriek

Abstract

Vapour deposited $Pt_xNi_yAl_z$ thin film electrocatalysts were evaluated for their activity towards the oxygen evolution reaction (OER) in alkaline medium (0.1 M KOH). An initial series of fifty-two $Pt_xNi_yAl_z$ thin films were sputtered, (employing physical vapour deposition), onto an electrical circuit on a Si/SiO_2 wafer for high-throughput electrocatalytic screening of these thin film electrocatalysts towards the OER. From this initial screening exercise, a refinement step was subsequently performed employing the most electro-active xyz-region exhibited. This refinement involved the generation of a new set of fifty-four $Pt_xNi_yAl_z$ thin films that were sputtered onto a second Si/SiO_2 wafer for further high-throughput electrocatalytic screening. From the screening of the refined ratios, the ten best performing ratios were sputtered onto 5 mm diameter glassy carbon (GC) electrode inserts for physical and electrochemical characterisation employing energy dispersive x-ray spectroscopy (EDX), linear sweep voltammetry (LSV), and chronopotentiometry (CP). Stoichiometric characterisation of these sputtered electrocatalyst thin films both prior to and subsequent to chronopotentiometry (CP) measurements revealed a marked difference between the theoretically generated ratios and the actual sputtered ratios. This was attributed to arching of the plasma between the different magnetrons inside the vacuum chamber of the physical vapour deposition apparatus. The ratios with the highest electrocatalytic activity towards the alkaline OER are $Pt_{12}Ni_{88}$, $Pt_{21}Ni_{47}Al_{32}$ and $Pt_{21}Ni_{54}Al_{25}$ requiring an overpotential of 335 mV, 337 mV and 337 mV to attain a current density of 10 $mA.cm^{-2}$ at 25 °C (subsequent to stability tests). $Pt_{21}Ni_{47}Al_{32}$ and $Pt_{21}Ni_{54}Al_{25}$ also exhibited the lowest Tafel slope values of 46.87 $mV.dec^{-1}$ and 46.46 $mV.dec^{-1}$ respectively. However, the most optimal electrocatalyst is $Pt_{14}Ni_{52}Al_{34}$, as it not only exhibited a low overpotential (350 mV) and the lowest Tafel slope (46.46 $mV.dec^{-1}$) after the binary $Pt_{12}Ni_{88}$ subsequent to durability testing. But it's also the ternary electrocatalyst with the lowest mass of Pt and Ni loading. Moreover, it exhibited the highest specific mass activity per Pt (139.40 $mA.cm^{-2}.\mu g\ Pt^{-1}$) and Ni loading (44.58 $mA.cm^{-2}.\mu g\ Ni^{-1}$) compared to the other sputtered electrocatalysts after durability testing. It has been shown that the activity towards

the alkaline OER can be substantially increased, compared to the activity of the individual components, i.e. pure Pt, pure Ni and pure Al, by combining Pt, Ni, and Al in a co-deposited thin metal film.

Introduction

Water electrolysis is an 'old' but promising technology for the production of hydrogen gas (H_2), which can be utilised for energy conversion and storage purposes [1-3]. It produces high purity hydrogen and is a pollution free-process when combined with renewable energy sources such as wind or solar [4, 5]. Although alkaline water electrolysis is a well-established technology, it promises great advancements to sustainable energy conversion and storage applications as it not only uses cheaper materials, but is being actively researched [6, 7]. The efficiency of this process is linked to the activity of the OER at the anode in both acidic (eq. 1) and basic medium (eq. 2) [8], as this is the limiting reaction due to its sluggish kinetics and high overpotentials [6, 9, 10].

$$2H_2O \rightarrow O_2 + 4H^+ + 4e^- \quad (1)$$

$$4OH^- \rightarrow O_2 + 2H_2O + 4e^- \quad (2)$$

As the OER is susceptible to the type and structure of the electrocatalysts employed, research has shown that in alkaline medium Ni-based spinels and perovskites are superior, whereas noble metal oxides such as RuO_2 and IrO_2 are the best electrocatalyst under acidic conditions [10-12]. RuO_2 and IrO_2 have been extensively studied and exhibit metal-like conductivity in both basic and acidic media, with RuO_2 being really active but less stable due to dissolution that occurs when it is slowly attacked by alkaline electrolytes resulting in loss in activity [12, 13]. In an attempt to improve the stability and corrosion resistance of these two electrocatalysts, RuO_2 and IrO_2 have been combined, which resulted in enhanced activity, however, a decrease in stability has been observed [12, 14]. The anode's dependence on expensive noble metal electrocatalysts, specifically for acidic or proton exchange membrane (PEM) water electrolysis, such as Ru and Ir has limited the large-scale use of this technology. Other noble metals that are less expensive than Ru and Ir such as Pt, Pd and Au, have been considered [14-16]. Platinum has been accepted as an excellent electrocatalyst for the oxygen reduction reaction (ORR) in fuel cells [17, 18], however, Pt exhibits poor activity for the OER. For this reason, researchers aim to look for bifunctional Pt-based electrocatalysts for water electrolysis [19]. Reports aimed at improving the OER catalytic properties show that oxide modified noble metals such as Pt-$CaMnO_3$ and Pt-TiO_2 exhibit high catalytic activity for OER [20-22]. Additionally, in an attempt to circumvent the extensive use of noble metal

electrocatalysts, extensive research has been undertaken for the development of effective OER electrocatalysts that exhibit both high activity and stability under harsh conditions [20]. A global criterion can therefore be set, which requires an ideal electrocatalyst to be of low cost, have long term stability against corrosion and have a low overpotential for the anodic OER. To this regard, Ni and Ni-based materials have been widely considered as they are less costly than noble metals, have good oxygen evolution electrocatalytic properties and are less prone to corrosion in strong alkali medium. This is evident from its use as a core material in bipolar electrodes for alkaline water electrolysers [6, 15, 16, 23]. The Ni-based materials used as stable electrocatalysts for the OER include spinels, perovskites and oxide/hydroxide layers [24]. Raney nickel (a nickel aluminium alloy) has also been reported as being an effective OER electrocatalyst and its activity results from the selective leaching of Al from the NiAl alloys resulting in a large active surface area and additional active sites that formed during the leaching of Al [25]. Although Raney nickel remains superior compared to elemental nickel for the OER, $NiCo_2O_4$, Ni-Fe and $NiFe(OH)_2$ are some of the bifunctional electrocatalysts that have also been used for the OER, due to their high electrocatalytic activity [26]. In their study of high surface area mixed Ni/Fe oxides, prepared by cathodic deposition and thermal methods, Xiahong Li *et al.* reported that $NiFe(OH)_2$ is a good electrocatalyst due to its low cost as well as its stability (tested over 10) days [24]. Furthermore, a study done on nickel-based composite coatings in alkaline media has shown that the apparent activity towards the OER of Ni + Mo and modified Ni + Mo_{Si} composite coatings is higher than that of Ni electrodes. This was observed to be caused by an apparent increase in the double layer capacitance, which occurred due to an increase in the electrochemical active surface area [27]. Even though not much research exists on the activity of Al for the OER, a study by Lee on the combination of Pt and Al towards aqueous SO_2 electro-oxidation, has shown that only a small amount of Al is needed to improve the electrocatalytic activity of the system [28]. This study was conducted in search of an optimal electrocatalyst in alkaline medium for the OER reaction for water electrolysis. Herein, we investigated the physical and electrochemical characterisation of several combination ratios of $Pt_xNi_yAl_z$ electrocatalysts that were sputtered as thin films on a Si-SiO_2 wafer and glassy carbon inserts (GC's) employing physical vapour deposition (PVD). Combinatorial and high-throughput PVD is a technique that facilitates screening of a large number of catalyst materials simultaneously to minimize the time consumed and reduce the number of experiments necessary to evaluate a catalyst's activity [26]. In this study, a simultaneous combination of Pt, Ni and Al was introduced in order to lower the content of the noble metal in the electrocatalyst. The OER activity and stability of the $Pt_xNi_yAl_z$ electrocatalysts were tested in alkaline medium using a combination of linear sweep voltammetry (LSV) and chronopotentiometry (CP) techniques.

Experimental

The thin films were deposited on the Si-SiO_2 wafers (100mm diameter, 500µm thickness, Microchemicals, Germany) and the GC's (GC, Sigradur G, HTW Germany) for screening and characterisation. Firstly, sixty-four ratios of $Pt_xNi_yAl_z$ (10% content increment) were generated using an Excel sheet, however, only 52 of the 64 generated ratios were sputtered onto the first Si-SiO_2 wafer. The remaining 12 ratios were not sputtered because they contained a high amount of Ni, and the sputtering time required is very high and would be time consuming. The two wafers were prepared, deposited and screened using the photolithography method described in the supplementary information (SI) document. The conditions for the PVD (Figure 1) of the 30 nm thick thin films and the specifications of the contact pads (0.09 cm^2) on the wafer are stated in Table 1. Once the deposition was completed, the wafer was screened using a high-throughput electrochemical screening cell (Figure 2). In this electrochemical cell, all 64 individual working electrodes on the wafer are connected to a 64-channel potentiostat (Arbin MSTAT). The electrochemical cell (Figure 2) and the process for the high-throughput screening on the wafer is fully described in the SI document. LSV's were performed on the wafer at a scan rate of 5 $mV.s^{-1}$ within the voltage range of 0.1 V – 0.8 V vs. Hg/HgO in a O_2-saturated 0.1M KOH solution. Using the results obtained from this wafer, 54 new $Pt_xNi_yAl_z$ ratios were generated (5% content increment) and sputtered as thin films on the second wafer. These 54 $Pt_xNi_yAl_z$ ratios were obtained from the most electroactive xyz-region exhibited by the thin films deposited on the first wafer. This was done to isolate the electroactive ratios and ultimately obtain the most active electrocatalyst. The second wafer was also screened employing the same high-throughput cell and the same LSV conditions. However, this wafer was subjected to three subsequent LSV scans in order to monitor any possible physical changes (dissolution/leaching) occurring on the thin films. The results obtained from these LSV's were used to identify the 10 most active electrocatalysts that were subsequently sputtered onto the GC's for further characterisation and testing. Energy dispersive X-ray spectroscopy (EDX, Xmax 20 Oxford Instruments) characterisation of the wafer could not be performed due the size of the wafer being too large to fit into the EDX apparatus, and breaking the wafer into smaller pieces would possibly damage the sputtered thin films. It was therefore decided that any possible changes of the electrocatalyst ratios, caused by dissolution or leaching, would rather be monitored on the GC's. The 10 most electroactive thin films were furthermore sputtered in triplicate onto the GC inserts (0.196 cm^2) that were used as substrates for further conventional electrochemical characterisation. This deposition of the thin films onto the GC's was done employing the conditions in Table 1.

Table 1. Conditions used for sputtering of the wafer

PVD specifications for sputtering		**Specifications of contact pads**	
Vacuum base pressure	5 x 10^{-7} Torr	Size of contact pad	3 x 3 mm
Chamber pressure	8 mTorr	Pad spacing	2.5 mm
Argon flow rate	0.015 L min^{-1}	Size of pin pad connecting pads to potentiostat	2.5 x 6 mm
		Spacing between pin pads	1 – 1.5 mm

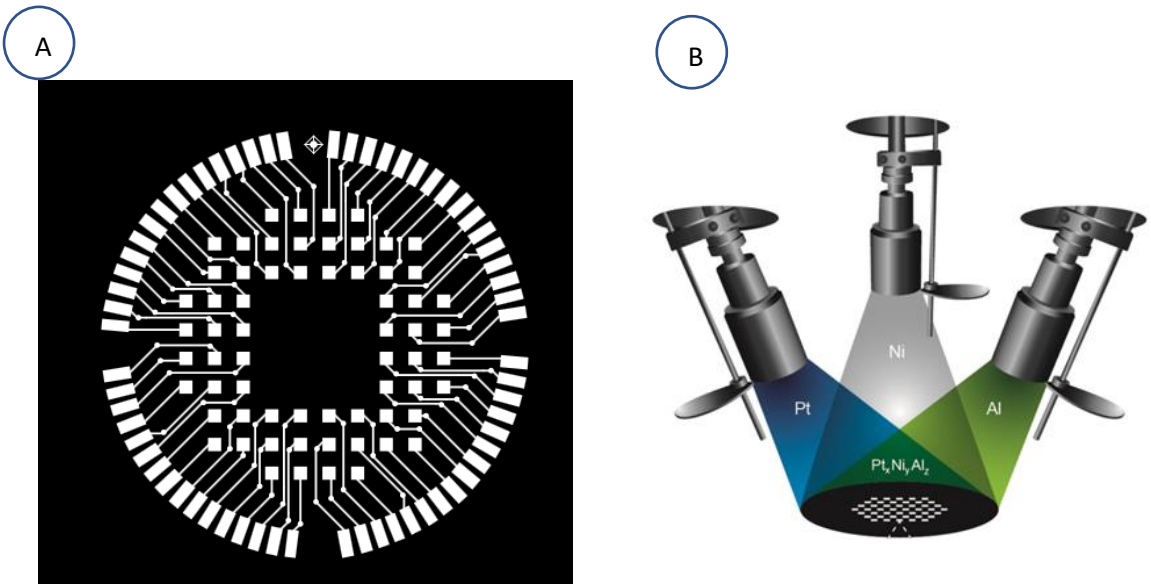

Figure 1. Circuit layout on Si-SiO_2 wafer (a) and the combinatorial PVD system used for vacuum sputtering of thin film electrocatalysts (b)

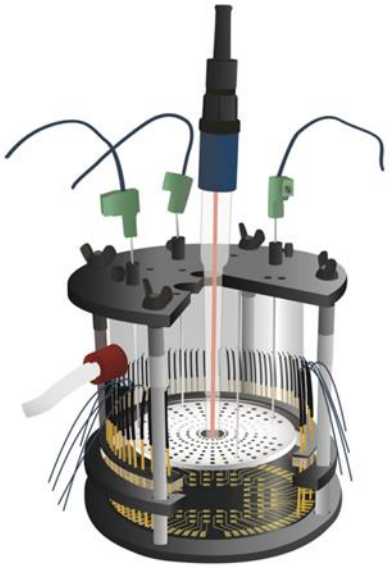

Figure 2. Schematic drawing of the in-house designed and manufactured electrochemical cell for high-throughput screening of combinatorial sputtered electrocatalysts on a Si-SiO_2 wafer (adapted from [41])

Before the Hg/HgO reference electrode (Radiometer) was used for electrochemical testing, it was first calibrated employing a method described by Chen and associates [44]. The Hg/HgO reference electrode was calibrated vs. RHE in a H_2-saturated 0.1M KOH solution. The potential was measured as being 0.929V vs. RHE using a WaveDriver 20 Bipotensiostat (Pine Research Instrumentation). Using the equation below, the potentials were IR-corrected:

$$E_{IR\ corrected} = E_{App} - IR$$

where R is the ohmic resistance of the cell and *I* is the current. The uncompensated ohmic resistance of the cell (41.20 Ω) was measured using an impedance measurement technique (ZIR) [29].

For the electrochemical measurements, linear sweep voltammetry (LSV) and chronopotentiometry (CP) techniques were performed using a conventional three electrode-setup in an electrochemical cell. A platinum spiral wire (Pine Research Instrumentation) was used as counter electrode and the previously calibrated Hg/HgO electrode served as the reference electrode. The working electrodes were the sputtered GC's with different electrocatalysts ($Pt_xNi_yAl_Z$). The different $Pt_xNi_yAl_Z$ thin film ratios sputtered onto the GC electrode inserts were employed as part of a rotating disk electrode (RDE) setup (Pine Research instrumentation), which served as the working electrode. The RDE reduces the

overpotential caused by oxygen bubbles that is formed on the electrocatalyst surface at high current densities and enhances mass transport of the active species from the bulk of the electrolyte solution to the surface [21, 30]. All LSV measurements were obtained using a WaveDriver 20 Bipotensiostat (Pine Research Instrumentation) with AfterMath software (version 1.25966). These electrochemical measurements were carried out under the same conditions, in 130 mL O_2-saturated (10 minutes) 0.1M KOH (Merck, uniVAR) at constant temperature of 25 °C (employing a Julabo F12-ED refrigerated thermostat) and a rotation rate of 1600 rpm in a potential window of 0.929 to 2.129V vs. RHE at a scan rate of 10 $mV.s^{-1}$. LSV of the thin films sputtered onto the GC's were conducted before and after the CP measurements under the stated conditions. Three repeats were performed for each electrocatalytic ratio and the mean LSV curve was used. CP was performed to test the stability/durability of the electrocatalysts on the GC's. Each electrocatalyst was subjected to a 10 hours CP scan at a constant current of 1.96 mA (this current represents the benchmark current density for OER electrocatalysts, i.e. 10 $mA.cm^{-2}$),130 ml O_2- saturated 0.1M KOH at constant temperature of 25 °C and a rotation rate of 1600 rpm. Structural characterization of the sputtered thin film electrocatalysts on the GC's was conducted before and after the electrochemical measurements using energy-dispersive X-ray spectroscopy (EDX, Xmax 20 Oxford Instruments).

Results and discussion

Wafer analysis

Linear sweep voltammetry (LSV) was employed to investigate the activity of the different electrocatalytic $Pt_xNi_yAl_z$ thin films sputtered onto the wafer for the OER. The LSV's obtained for the sputtered thin films are illustrated in Figure 3. The activity of all the generated electrocatalytic ratios obtained from the LSV's is represented in Figure 4. This ternary diagram was plotted by employing the currents (mA) exhibited by all the electrocatalytic ratios at a potential of 1.65 V vs. RHE. This is the potential on the LSVs right before the noise (caused by the accumulation of oxygen bubbles on the surface of the electrode surface since this system cannot be rotated) is observed. At this potential the overpotential caused by the presence of oxygen bubbles is, furthermore, minimised. On the ternary diagram, the red area indicates the electrocatalytic ratios with the highest electrocatalytic activity and the blue area indicates the lowest activity. In this area we observe that the highest activity is exhibited by electrocatalytic ratios containing: Pt and Al < 40% and Ni > 50%. The activity of these metal electrocatalysts for the OER in alkaline solution can be attributed to the intrinsic electrocatalytic properties of Ni in alkaline conditions, where literature state that Ni is a

relatively good electrocatalyst for the OER as it exhibits relatively low overpotentials and it is resistant to corrosion [8]. The lowest activity is observed from electrocatalysts with very little Ni content and very high Al content. Pure Pt and pure Al show very little activity in comparison to most ternary electrocatalysts as shown in Fig. 4, which is due to their poor intrinsic electrocatalytic properties for the OER in alkaline medium [19, 25, 26].

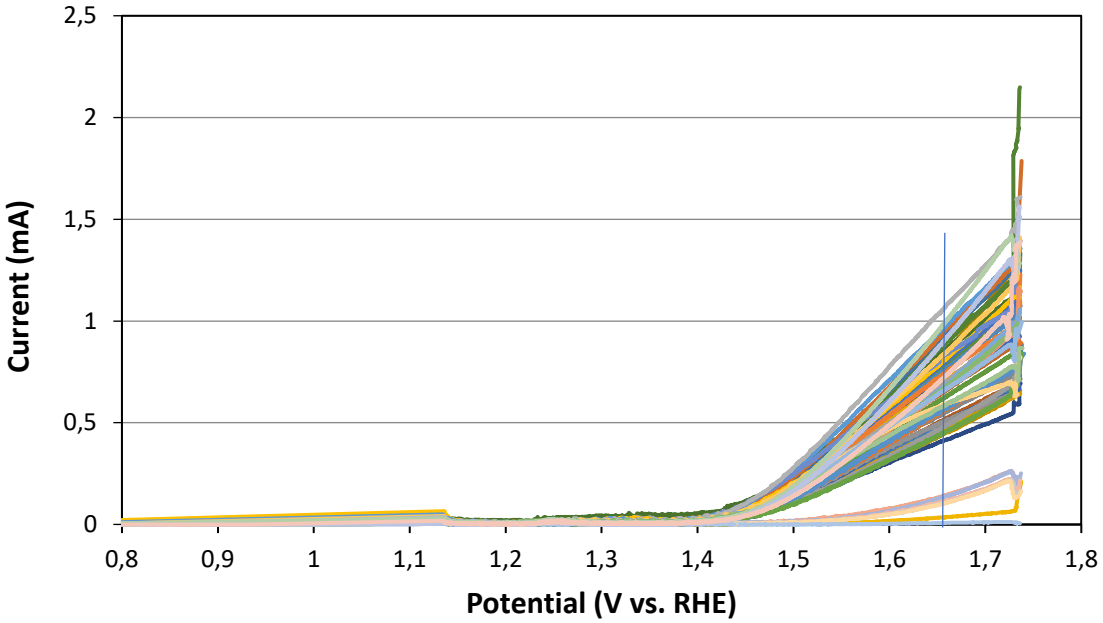

Figure 3. LSV's obtained for the 52 initially generated $Pt_xNi_yAl_z$ ratios sputtered on the SiO_2-wafer in 0.1M KOH electrolyte at a scan rate of 5 $mV.s^{-1}$ and 25 °C

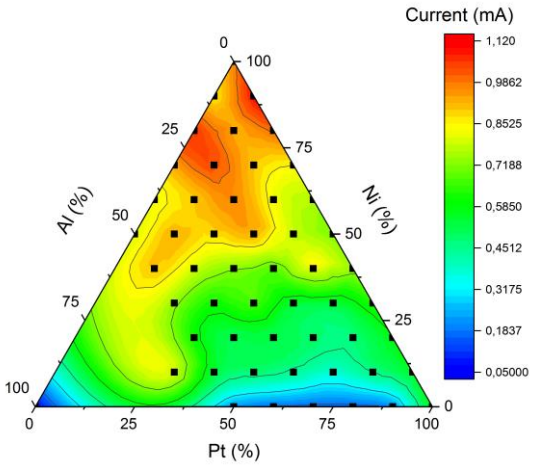

Figure 4. Ternary plot illustrating the currents obtained for the 52 generated $Pt_xNi_yAl_z$ ratios sputtered on the SiO_2-wafer in 0.1M KOH electrolyte at a scan rate of 5 $mV.s^{-1}$ and 25 °C

A subsequent refinement was conducted by sputtering 54 ratios of $Pt_xNi_yAl_z$ employing 5% increments within the region Pt ≤ 45%, Ni ≥ 55% and Al ≤ 45%, which was aimed at zooming in to try and identify the most optimum electroactive ratio. From this refinement (Fig. 5: A-C) it was observed there is a shift in the region of highest electrocatalytic activity, with the most active region (red spot) evolving in a region that is lower with regard to Ni, only slightly lower with regard to Pt, but higher with regard to Al (when comparing Fig 5: C to Fig 5: A). This shift in electrocatalytic activity appears to be due to a change that occurs in the composition of the electrocatalysts. One possible explanation for this outcome, could be leaching of Al from the $Pt_xNi_yAl_z$ matrix, which has been observed in literature and resulted in the improvement of the activity of NiAl electrocatalyst whereby the leaching of Al resulted in a larger active surface area and an increase in active sites [25, 26]. Similarly, in a study on the electrocatalytic behaviour of Ni-doped Mn_3O_4, an observation was made that the OER electrocatalytic activity increased with respect to the number of cyclic voltammetry scans when anodic current was taken into account [19]. This effect has been attributed to the possible formation of localised metal oxides and metal oxyhydroxides as a result of potential cycling during contact with the electrolyte in comparison to the initial material that had no contact with the electrolyte and did not experience any potential cycling [8, 19, 31]. This same effect could be what is observed on our ternary plots (Figure 5), an improvement in the electrocatalytic activity on the second and third run, which is caused by either a region becoming more active or the region of the activity shifting due to leaching that occurs and thereby changing the ratios. However, this speculation will be further investigated through additional using further electrochemical characterisation conducted on the vapour deposited GC's. Other research has shown that Ni-M_x (M_x = metal) tends to oxidise during the OER, which could also be the reason for the observed change in electrocatalytic activity of the generated ratios in subsequent electrochemical LSV's [6, 32]. In the second and third run, the metal catalysts have already oxidised and therefore exhibit a higher activity than the first run, which can be attributed to the accepted fact that Ni-oxides exhibit higher electrocatalytic activity as it forms Ni-oxy-hydroxides (NiOOH) through oxidation (Eq 1-4) [32, 33]. The superscript '*' denotes the surface absorbed species.

$$OH^- \rightarrow OH^* + e^- \quad (1)$$

$$OH^- + HO^* \rightarrow O^* + H_2O + e^- \quad (2)$$

$$OH^- + O^* \rightarrow OOH^* + e^- \quad (3)$$

$$OH^- + 2OOH^* \rightarrow OOH^* + H_2O + O_2 + e^- \quad (4)$$

The overall reaction is $4OH^- \rightarrow O_2\uparrow + 2H_2O + 4e^-$. For the OER in alkaline solution, the activity of the metal electrocatalyst can be attributed to the adsorption of OH^- ions on the surface of the metal atoms [34]. This adsorption process facilitates the electron transfer process where two adsorbed oxygen atoms combine to produce an O_2 via the intermediates of metal-OH (M-OH) or metal- hydroperoxo species (M-OOH) [19, 29]

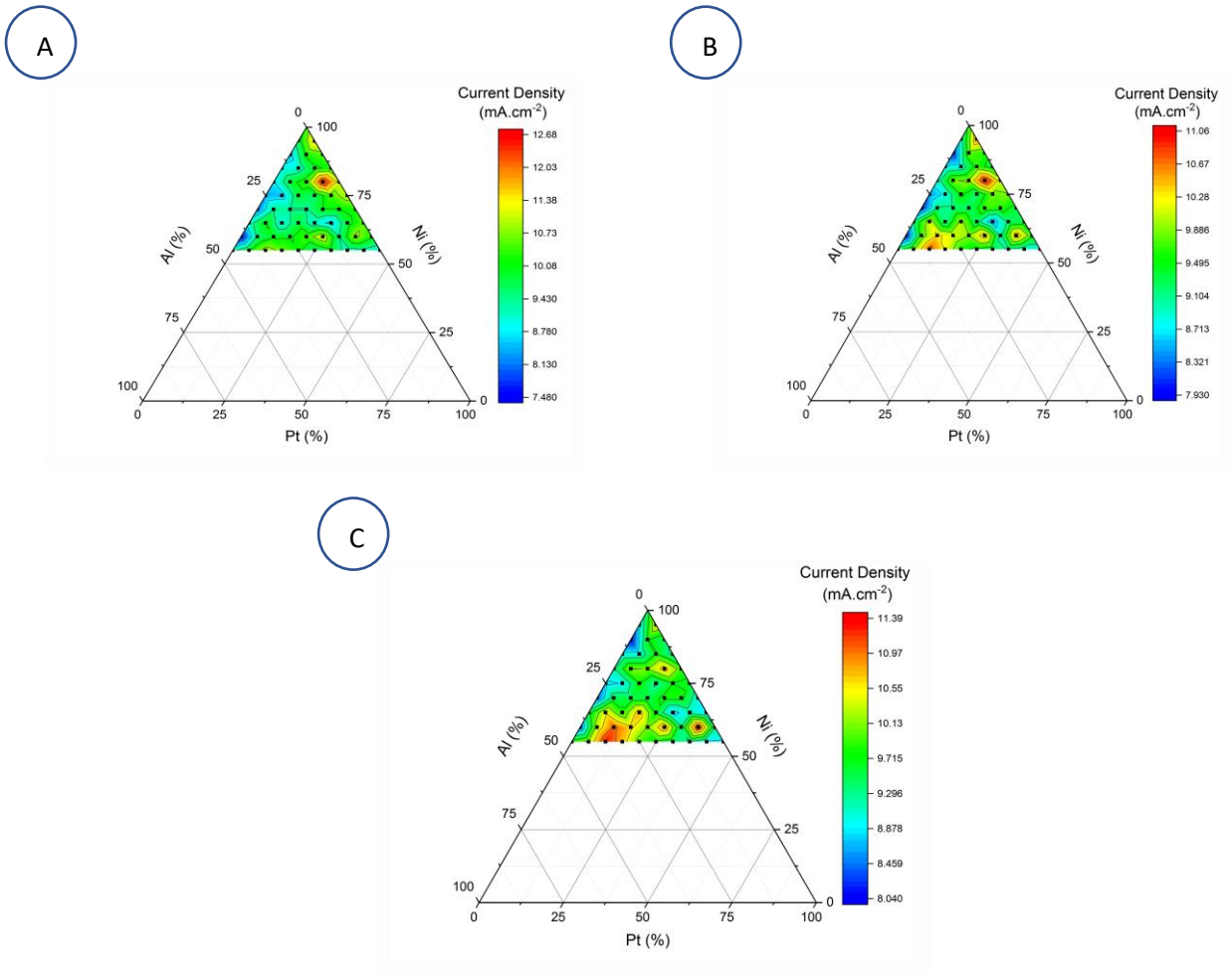

Figure 5. Ternary plots illustrating the current densities obtained from the 54 refined ratios of the subsequent (a) first LSV, (b) second LSV and (c) third LSV

Electrochemical characterisation on GC's

The stoichiometry of the ten-best sputtered $Pt_xNi_yAl_z$ thin film ratios was confirmed employing EDX with the results presented in Table 2.

Table 2: EDX analysis of constituent elements for the ten best electrocatalytic ratios

Theoretically sample	**Label**	**Atomic% (Before CP)**			**Atomic% (After CP)**		
		Pt	**Ni**	**Al**	**Pt**	**Ni**	**Al**
Ni_{100}		-	100	-	-	100	-
Pt_5Ni_{95}	A	12	88	-	12	88	-
$Pt_{15}Ni_{80}Al_5$	B	21	70	9	26	66	7
$Pt_{15}Ni_{65}Al_{20}$	C	23	55	22	24	55	21
$Pt_{10}Ni_{60}Al_{30}$	D	14	52	34	12	52	36
$Pt_{15}Ni_{60}Al_{25}$	E	21	54	25	26	52	22
$Pt_{25}Ni_{60}Al_{15}$	F	34	49	17	42	44	15
$Pt_{35}Ni_{60}Al_5$	G	44	49	7	45	48	7
$Pt_{10}Ni_{55}Al_{35}$	H	16	46	38	13	48	39
$Pt_{15}Ni_{55}Al_{30}$	I	21	47	32	14	49	37

Inspection of the EDX results obtained for the sputtered ratios (before CP testing) highlights the fact that there is a discrepancy in the actual stoichiometry compared to that of the theoretical $Pt_xNi_yAl_z$ ratio. The actual amount of Ni sputtered on the pad is about 10 % less than the theoretical amount, with Pt and Al on the other hand being about 5% greater than the theoretical amount. During magnetron sputtering, the magnetic leakage flux (MLF) must be approximately 150 gauss at the target surface under normal sputtering conditions (with an argon pressure of 5-10 mTorr) to start and sustain the plasma. This MLF is determined by the magnet strength of the cathode sputtering target. The higher the magnet strength, the higher

the MLF. However, in the case of ferromagnetic metals such as nickel, there is a reduced MLF on the target. This is caused by the high intrinsic magnet permeability of the nickel, which shields the magnetic field from the magnets behind the target. As a result of the reduced MLF, there is a reduced sputtering efficiency for nickel. Hence, we observe a lower amount of nickel being sputtered compared to the initial theoretical amount [35]. Another possible reason for the discrepancies observed is the fact that the calibration of the PVD is done using one metal at a time. However, co-sputtering (simultaneous sputtering of Pt, Ni and Al) is done of the electrocatalysts and the possible effects originating from co-sputtering is not taken into account when calibrating the metals. The sputtering process is closely related to the thin film produced on the GC, to this regard, Kinbara shows in his study that there are a number of factors that affect the character of the sputtered thin film, which is the reason why the structure and properties on the thin films are difficult to control [36].

Moreover, EDX performed on the GC's subsequent to CP testing shows a slight change from the initial composition of the sputtered ratios. An inconsistent change in the composition of the electrocatalysts are observed subsequent to CP testing. This change appears to correlate with the observation on the second wafer, as part of the refinement study, as a shift was observed with regards to the active region (Figure 5), which can be attributed to a change in composition as a result of the second and third LSVs. This same change can explain the difference observed in the EDX readings on the GC's before and after CP testing. The composition of the electrocatalytic thin films change as a result of the applied potential with most of the electrocatalysts gaining activity subsequent to the application of potential.

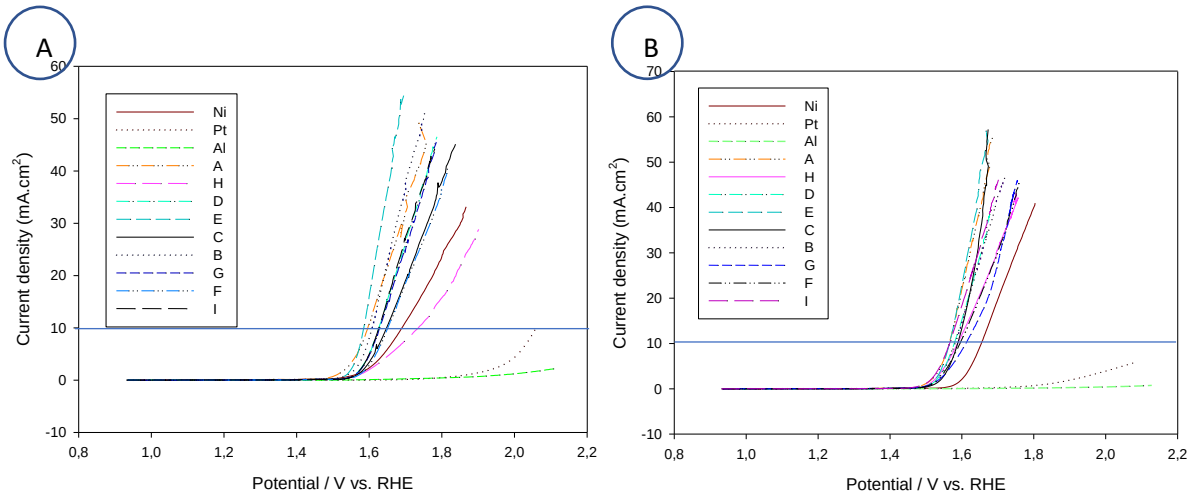

Figure 6. (a) LSV's obtained for the 10 most active electrocatalysts before CP testing, and (b) LSV's of the best 10 electrocatalysts after CP testing

In comparison to the other bimetallic and trimetallic electrocatalysts, pure Pt and Al are seen (Figure 6a and b) to exhibit the lowest activities by far, and they furthermore do not achieve

the benchmark current density of 10 mA.cm^{-2} neither before nor after the CP tests. Their activities are furthermore seen to drastically decrease subsequent to CP testing, which are attributed to the dissolution of the sputtered thin films on the GC's. This shows that both pure Pt and Al are not desirable electrocatalysts by any means. Conversely, an increase in electroactive activity is observed in most of the other electrocatalyst subsequent to the stability testing. The onset potential on the LSV curves moves to the left (thus creating a steeper LSV curve), therefore lowering the overpotential towards the OER. This appears to be in correlation with the observation made on the screening of the second wafer (Figure 5), which clearly showed that the activity of these electrocatalysts improve with time in response to applied potential. This observation, that the combination of Ni with one or two other metals improve the electrocatalytic activity, is supported by Sapountzi's research who reported that (for the OER) an addition of a second metal to Ni has shown to significantly improve the activity of the electrocatalyst [6].The overpotentials for the ten GC samples, before and after the CP testing, are presented in the following ternary plots (Figure 7a and b), with the most active electrocatalysts, i.e. having the lowest overpotential shown in blue. Available research shows that individual metals such as Pt and Al are electrocatalytically inferior to Ni [37], and this is evident in the fact that Pt and Al in these experiments exhibited no overpotential at 10 mA.cm^{-2}. $Pt_{12}Ni_{88}$ requires an overpotential of 335 mV, $Pt_{21}Ni_{54}Al_{25}$ 337 mV and $Pt_{21}Ni_{47}Al_{32}$ 337 mV after CP tests. These three electrochemical ratios appear to have the most active electrocatalytic activity from the sputtered ternary electrocatalysts and even compared to pure Ni which required an overpotential of 384 mV after CP testing to reach a current density of 10 mA.cm^{-2}. Electrocatalysts $Pt_{12}Ni_{88}$, $Pt_{14}Ni_{52}Al_{34}$ and $Pt_{21}Ni_{54}Al_{25}$ from these experiments also show low overpotentials in comparison to the benchmark electrocatalysts for OER (in acidic medium) RuO_2 (380 mV) and IrO_2 (380 mV) as reported by Jung and associates [38]. $Pt_{21}Ni_{47}Al_{32}$, $Pt_{21}Ni_{54}Al_{25}$, exhibit the lowest overall overpotential after the bimetallic $Pt_{12}Ni_{88}$ and have quite similar compositions. The similarity in compositions can be an indication that further refinement (from 10 % to 5% content increment) of the initial active xyz-region was not really necessary because the two electrocatalysts 5% content increment apart show the same activity. However, considering our search for the most optimum electrocatalytic ratio, the refinement remains a significant part of our research. In addition to overpotential as a kinetic criteria, Tafel plots were also employed to further analyse the electrode kinetics related to each electrocatalyst for the OER. This was obtained by fitting the LSV curves for the Tafel equation, i.e. $\eta = b\ (\log i) + a$, where, η is the overpotential (V), b is the Tafel slope (mV.dec^{-1}), i is the experimental current density (mA.cm^{-2}) and a is a constant. These Tafel plots are shown in the SI document (Figure S3a and b), however the values obtained are illustrated in the ternary plots in Figure 8. The Tafel slope values calculated for the electrocatalysts are displayed with the lowest value shown in blue, which indicate the highest activity. The lowest

Tafel slope has been exhibited by $Pt_{21}Ni_{54}Al_{25}$ (44.79 mV.dec^{-1}) and points towards favourable electrode kinetics and improved electrocatalytic activity compared to pure Ni. The Tafel plot values for $Pt_{21}Ni_{54}Al_{25}$ (44.79 mV.dec^{-1}), $Pt_{14}Ni_{52}Al_{34}$ (46.46 mV.dec^{-1}) and $Pt_{21}Ni_{47}Al_{32}$ (46.87 mV.dec^{-1}) are comparatively lower than that of the benchmark noble metal oxide electrocatalysts for OER (in acidic medium): RuO_2 (47.7 mV.dec^{-1}) and IrO_2 (64.6 mV.dec^{-1}) [38]. Additionally, water oxidation is known to have multiple mechanisms with different determining steps because of the complex reaction pathways and four electron transfers. It therefore has different Tafel slope values 120, 40, 60 and 15 mV dec^{-1} [10]. Our electrocatalysts, $Pt_{21}Ni_{54}Al_{25}$, $Pt_{14}Ni_{52}Al_{34}$ and $Pt_{21}Ni_{47}Al_{32}$ exhibit Tafel slope values close to the value (40 mV dec^{-1}), suggesting that the low Tafel slopes of the aforementioned electrocatalysts indicate reduced kinetic overpotential losses. This can be attributed to the increase of bond strength for OH-adsorption on the $Pt_xNi_yAl_z$ electrocatalyst, which accelerates the rate of the electron reaction ($M + OH^- \rightleftharpoons MOH + e^-$) and improves electrocatalytic kinetics [10].

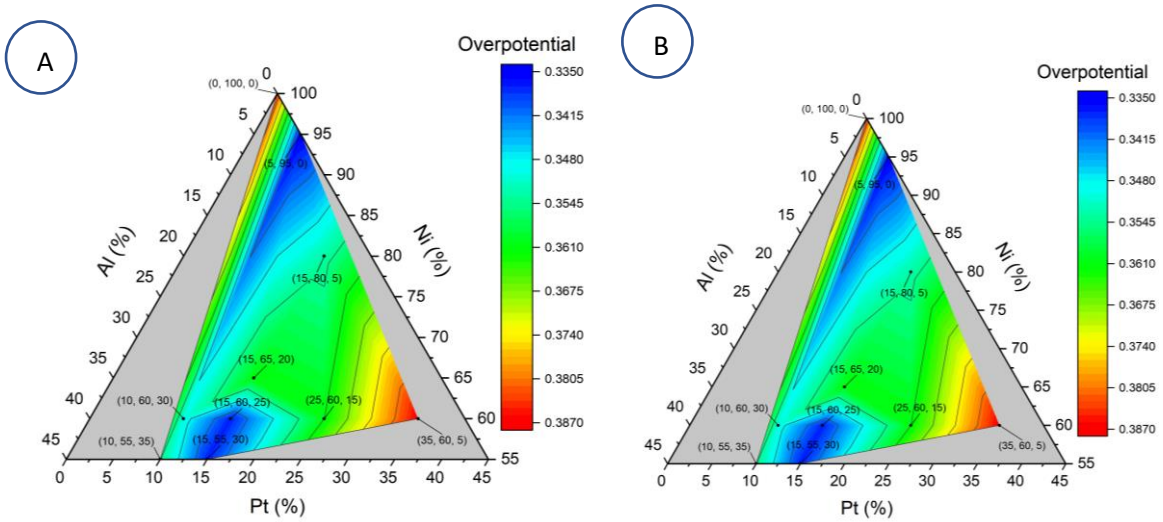

Figure 7. Ternary plots illustrating the overpotentials of the 10 GC sputtered electrocatalysts at 10 mA.cm^{-2} in 0.1 M KOH electrolyte at 10 mV. s^{-1} and 25°C, (a) before and (b) after CP testing

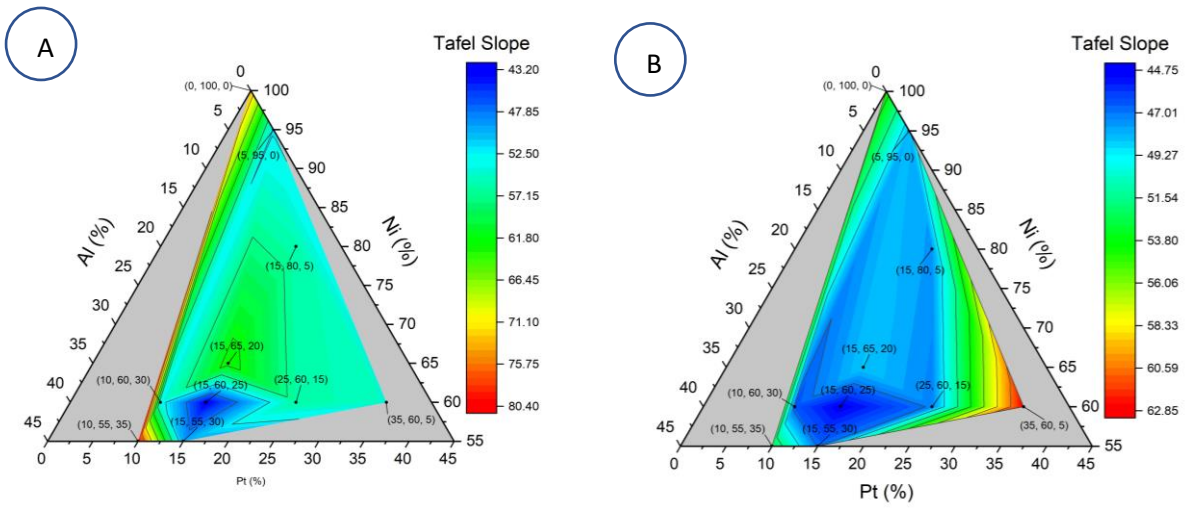

Figure 8. Ternary plots illustrating the Tafel slopes of the 10 GC sputtered electrocatalysts at 10 mA.cm^{-2} in 0.1 M KOH electrolyte at 10 mV. s^{-1} and 25 °C, (a) before and (b) after CP testing

The stability and short term durability of all the sputtered electrocatalyts were assessed employing CP measurements, subsequent to the initial LSV scan, at 10 mA.cm^{-2} (an applied current of 1.96 mA), at 25 °C and 1600 rpm for 10 hours (Figure 9). The electrocatalysts were compared against a clean unsputtered GC to observe any delamination and/or complete leaching of the sputtered electrocatalysts from the GC. Both Pt and Al are seen to be completely delaminated within 2 hours of the CP measurements. This shows that both Pt and Al alone are not durable electrocatalysts for the OER in alkaline medium as they not only exhibit very low electrocatalytic activity but are also not stable and/or durable. This was proven after 3 consecutive repeats of each electrocatalyst. Conversely, electrocatalysts containing combinations of $Pt_xNi_yAl_z$ show greater stability, which is observed from the CP plots exhibiting an almost horizontal line throughout the 10-hour period. Only sample H ($Pt_{44}Ni_{49}Al_7$) exhibited a slightly higher potential than the rest of the electrocatalysts, which could be attributed to selective leaching and/or oxidative degradation of the electrocatalytic layer [29]. However, this phenomenon hasn't been explored further. The mass specific activity, i.e. current density per Pt and Ni loading, of the electrocatalysts were calculated and compared. This was aimed at identifying an electrocatalyst that has a low amount of Pt loading (noble metal content) and exhibits high mass specific activity. Theoretically, the mass specific activity of a $Pt_xNi_yAl_z$ electrocatalyst is inversively proportional to the mass of Pt or Ni loading. In Figure 10a, we observe an increase in mass specific activity of the majority of the sputtered electrocatalyst, specifically with Sample D ($Pt_{14}Ni_{52}Al_{34}$) that has the lowest mass of pt loading (µg Pt) exhibiting the highest specific mass activity subsequent to the durability testing. Since there is not a significant change observed in the composition of the catalyst (as supported by EDX

results in table 2), this increase in activity can be attributed to Al leaching in the solution as a potential is applied, which causes openings and pores on the surface of the catalysts, which results in a more active surface area [25]. As expected, Pt exhibits the lowest specific mass activity prior to the durability tests and shows no activity subsequent to the durability testing as it completely delaminated. This observation substantiates the fact that Pt alone is not an OER electrocatalyst. In Figure 10b, The samples with the highest mass of Ni loading (Ni and sample G ($Pt_{44}Ni_{49}Al_7$)) exhibit the lowest mass specific activities before and after CP measurements. This shows us that although Ni is a preferred OER catalyst[6], on its own, it does not perform better than the sputtered ternary $Pt_xNi_yAl_z$ compositions. Sample D ($Pt_{14}Ni_{52}Al_{34}$) contains the lowest mass of sputtered Ni, exhibits the highest mass specific activity prior and subsequent to durability testing. The mass of Pt (µg Pt) and Ni (µg Ni) sputtered of the $Pt_xNi_yA_z$ electrocatalytic ratios are provided in the SI document (Table S2 and S3).

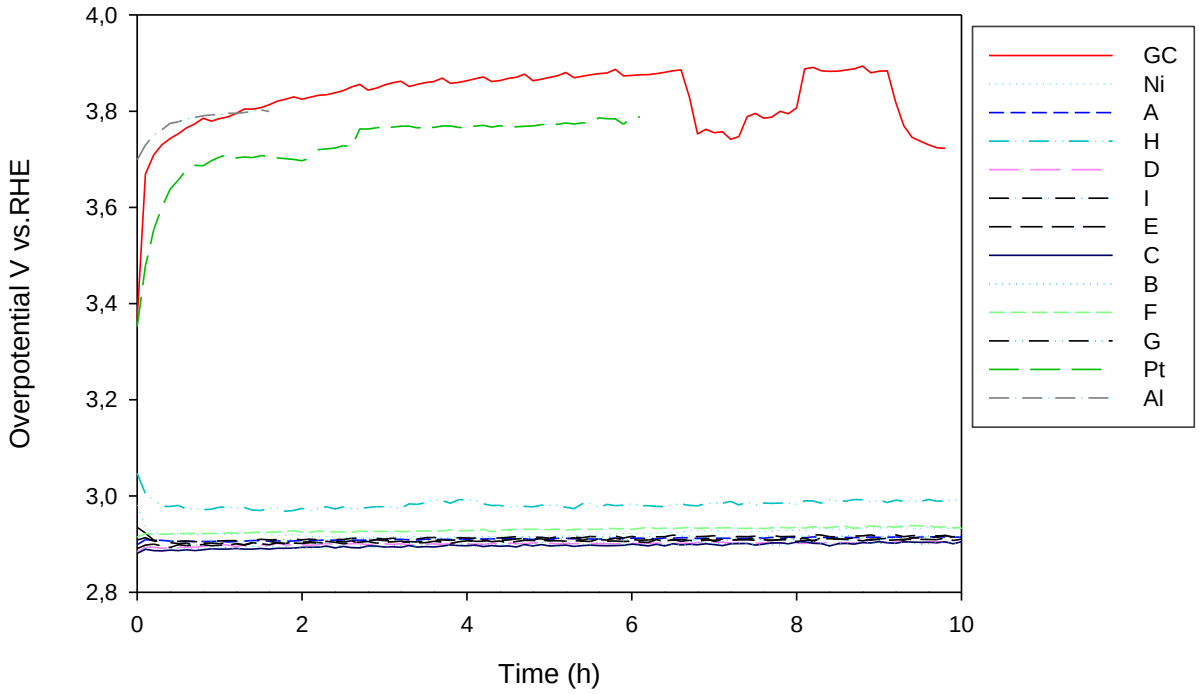

Figure 9. Chronopotentiometry (CP) plots attesting to the durability of the $Pt_xNi_yAl_z$ electrocatalysts (recorded at 10 $mA.cm^{-2}$ at 1600 rpm and 25 °C)

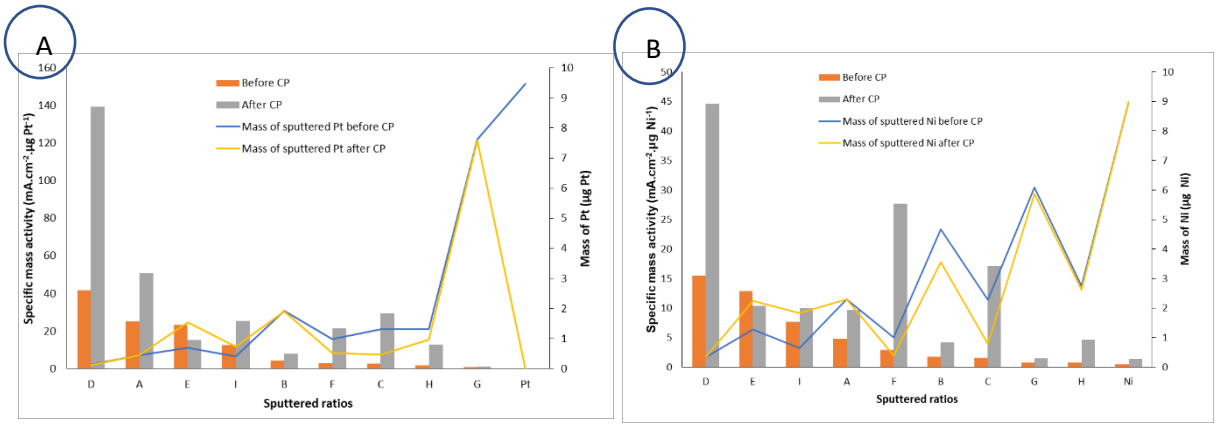

Figure 10. Mass specific activity per (a) Pt and (b) Ni loading on the electrocatalysts before and after CP testing

A complete illustration of the key kinetic parameters used to compare the activities of the $Pt_xNi_yAl_z$ electrocatalysts sputtered for this study is summarised in Table 3. This study was aimed at identifying a $Pt_xNi_yAl_z$ electrocatalytic thin film for the OER in alkaline medium. However, the combination of Ni_yAl_z wasn't explored past the Si-SiO_2 wafer stage as it did not exhibit significant activity compared to the selected 10 electrocatalysts. Results illustrated in Table 3 confirm that Pt is not an active OER catalyst as it did not reach 10 $mAcm^{-2}$ under the studied potential range. Ni on the hand is a preferred catalyst for OER in alkaline medium, however, compared to the other selected ternary electrocatalysts, it exhibited poor activity in terms of overpotential (384 mV after durability testing) at 10 $mAcm^{-2}$. Ni also, exhibited poor mass specific activity compared to the other electrocatalyst even though it contained the highest mass per Ni loading. Evidently, the bimetallic $Pt_{12}Ni_{88}$ is a good performing electrocatalyst for the OER as it exhibits the lowest overpotential (335 mV) after durability testing, a low Tafel value of 48.19 $mV.dec^{-1}$ and its mass specific activities (both per Pt and Ni loading) are seen to significantly increase subsequent to the durability testing (indicating a low amount of Pt content in the catalyst). However, $Pt_{21}Ni_{54}Al_{25}$ is seen to maintain consistent satisfactory electrocatalytic activity before and after the durability testing. This sample shows competitive activity to $Pt_{12}Ni_{88}$ as it exhibits the lowest overpotential (356 mV) before CP and even lower overpotential after the durability test (337 mV). The increase in activity of $Pt_{21}Ni_{54}Al_{25}$ subsequent to the durability test is attributed to the leaching of Al in alkaline medium, which leads to formations of pores and voids that increase the surface area, which in turn provide improved activity [2, 25]. However, the mass specific activity drops from 23.34 to 15.09 $mA.cm^{-2}.\mu g\ Pt^{-1}$ for this sample subsequent to the durability test as we observe an increase in the mass of Pt loading (this is supported by the EDX values in table 2). Sample D ($Pt_{14}Ni_{52}Al_{34}$), is the ternary electrocatalyst with the lowest mass of Pt and Ni loading, exhibiting a low overpotential (350 mV) and the lowest Tafel slope (46.46 $mV.dec^{-1}$) after the binary

$Pt_{12}Ni_{88}$ subsequent to duraibility testing. This electrocatalyst exhibits the highest mass specific activity per Pt and Ni loading compared to the other sputtered electrocatalysts bothe before and after durability testing.

Table 3: Overall kinetic parameters used in this study to evaluate the sputtered $Pt_xNi_yAl_z$ electrocatalysts

Label	Actual sample	Overpotential (mV) @ 10 mA.cm^{-2}		Tafel slopes (mV.dec^{-1})		Mass specific activity per Pt loading (mA.cm^{-2}.µg Pt^{-1})		Mass specific activity per Ni loading (mA.cm^{-2}.µg Ni^{-1})	
		Before CP	After CP	Before CP	After CP	Before CP	After CP	Before cp	After CP
A	$Pt_{12}Ni_{88}$	375	335	52.21	48.19	25.08	50.88	4.78	9.69
E	$Pt_{21}Ni_{54}Al_{25}$	356	337	43.30	44.79	23.34	15.09	12.90	10.37
I	$Pt_{21}Ni_{47}Al_{32}$	397	337	49.61	46.87	12.39	25.29	7.73	10.02
D	$Pt_{14}Ni_{52}Al_{34}$	399	350	53.67	46.46	41.75	139.40	15.54	44.58
B	$Pt_{21}Ni_{70}Al_{9}$	378	353	55.87	47.64	4.28	7.89	1.77	4.21
H	$Pt_{16}Ni_{46}Al_{38}$	499	355	80.36	52.93	1.63	12.66	0.78	4.64
C	$Pt_{23}Ni_{55}Al_{22}$	432	361	62.97	48.56	2.71	29.25	1.56	17.14
F	$Pt_{34}Ni_{49}Al_{17}$	425	361	56.27	47.18	3.06	21.30	2.97	27.68
Ni	Ni_{100}	452	384	73.32	54.44	-	-	0.54	1.43
G	$Pt_{44}Ni_{49}Al_{7}$	391	387	54.69	62.82	0.65	1.13	0.82	1.46
Pt	Pt_{100}	-	-	-	-	0.0045	-	-	-

Conclusion

In this study, we successfully sputtered a number of $Pt_xNi_yAl_z$ electrocatalytic thin films employing a sputtering PVD equipment and tested them for the OER in alkaline medium. The composition of the electrocatalyst thin films were elucidated employing EDX prior and subsequent to durability testing. Pure Pt and Al proved to be poor electrocatalysts for the OER in alkaline medium. Pure Ni did not show any satisfactory activity when compared to the 9 selected $Pt_xNi_yAl_z$ electrocatalysts. However, under the same conditions the combination of Pt, Ni and Al forming a trimetallic $Pt_xNi_yAl_z$ or bimetallic Ni_yAl_z significantly increased the activity and stability for the OER in alkaline medium. The presence of Ni and Al, decreased the noble metal Pt % required for the OER electrocatalyst and also improved its activity and stability towards corrosion and delamination. $Pt_{12}Ni_{88}$ required an overpotential of 335 mV, $Pt_{21}Ni_{47}Al_{32}$

and $Pt_{21}Ni_{54}Al_{25}$ respectively, exhibited the lowest overpotential (337 mV) from all the generated trimetallic electrocatalysts with a current density of 10 $mA.cm^{-2}$ and the lowest Tafel slopes of 46.87 $mV.dec^{-1}$ and 44.79 $mV.dec^{-1}$. However, the most optimal electrocatalyst is $Pt_{14}Ni_{52}Al_{34}$, as it's the ternary electrocatalyst with the lowest mass of Pt and Ni loading, exhibiting a low overpotential (350 mV) and the lowest Tafel slope (46.46 $mV.dec^{-1}$) after the binary $Pt_{12}Ni_{88}$ subsequent to durability testing. This electrocatalyst exhibits the highest mass specific activity per Pt and Ni loading compared to the other sputtered electrocatalysts both before and after durability testing. The slight discrepancy between the generated ratios and the actual sputtered ratios as thin films cannot be ignored and demands further investigation on the PVD equipment.

Recommendations

The results obtained in this study gives us a clear indication that the activity towards the OER can indeed be further improved using the right electrocatalyst. However, much research remains to be done on $Pt_xNi_yAl_z$ electrocatalysts as thin films. Firstly, the calibration of the PVD metal targets should be done on all metals simultaneously and not one metal at a time as this could have an impact on the accuracy of the compositions sputtered. This will account for the possible magnetic effect of each metal and reducing the discrepancies between the theoretical ratios and actual sputtered ratios. Secondly, physical and structural characterisation of the surface layer of atoms on these sputtered thin films must be done in greater detail, this will give a clear understanding of how they relate to the activity and stability since the active sites of the electrocatalyst are on the surface where the reaction takes place. Furthermore, the surface structure will enable the determination of ECSA, which would result in more accurate calculations of the kinetic parameters of the sputtered electrocatalysts.

References

1. M. Vanags , J. Kleperis, G. Bajars, A. Lusis, *Water electrolysis using electrodes with modified surface/volume.* Journal of Physics: Conference Series, 2007. **93**: p. 012025.
2. C.K. Kjartansdóttir, L.P. Nielsen and P. Møller, *Development of durable and efficient electrodes for large-scale alkaline water electrolysis.* International Journal of Hydrogen Energy, 2013. **38**(20): p. 8221-8231.
3. K. Zeng and D. Zhang, *Recent progress in alkaline water electrolysis for hydrogen production and applications.* Progress in Energy and Combustion Science, 2010. **36**(3): p. 307-326.
4. MD. Mamoon Rahid, M.K. Al Mesfer, H. Naseem and M. Danish, *Hydrogen Production by Water Electrolysis A review of alkaline water electrolysis, PEM, and high*

temperature water electrolysis. Internationl Journal of Engineering and Advanced Technology, 2015. **4**(3): p. 80-93.

5. D.M. Santos, A.C. Sequeira and J.L. Figueiredo, *Hydrogen production by alkaline water electrolysis.* Quimica Nova, 2013. **36**(8): p. 1176-1193.
6. F.M. Sapountzi, J.M. Gracia, C.J. Weststrate, HO.A. Fredriksson and J.W. Niemantsverdriet, *Electrocatalysts for the generation of hydrogen, oxygen and synthesis gas.* Progress in Energy and Combustion Science, 2017. **58**: p. 1-35.
7. P. Millet and S. Grigoriev, *Water Electrolysis Technologies.* 2013: p. 19-41.
8. M.S. Burke, M.G. Kast, L. Trotochaud, A.M. Smith and S.W. Boettcher, *Oxygen Evolution Reaction Electrocatalysis on Transition Metal Oxides and (Oxy)hydroxides: Activity Trends and Design Principles.* Chemistry of Materials, 2015. **27**(22): p. 7549-7558.
9. S. Ghosh and R.N. Basu, *Multifunctional nanostructured electrocatalysts for energy conversion and storage: current status and perspectives.* Nanoscale, 2018. **10**(24): p. 11241-11280.
10. G.Li, L. Anderson, Y. Chen, M. Pan and P.A. Chuang *New insights into evaluating catalyst activity and stability for oxygen evolution reactions in alkaline media.* Sustainable Energy & Fuels, 2018. **2**(1): p. 237-251.
11. B.M. Jović, U.C. Lacnjevac, V.D. Jovic and N.V. Krstajic, *Kinetics of the oxygen evolution reaction on NiSn electrodes in alkaline solutions.* Journal of Electroanalytical Chemistry, 2015. **754**: p. 100-108.
12. S. Cherevko, S. Geiger, O. Kasian, N. Kulyk, J-P. Grote, A. Savan, B.R. Shrestha, S. Merzlikin, B. Breitbach, A. Ludwig and K.J.J Mayrhofer, *Oxygen and hydrogen evolution reactions on Ru, RuO_2 , Ir, and IrO_2 thin film electrodes in acidic and alkaline electrolytes: A comparative study on activity and stability.* Catalysis Today, 2016. **262**: p. 170-180.
13. R.L. Doyle and M.E.G. Lyons, *The Oxygen Evolution Reaction: Mechanistic Concepts and Catalyst Design.* 2016: p. 41-104.
14. J. Lee, B. Jeong and J.D. Ocon, *Oxygen electrocatalysis in chemical energy conversion and storage technologies.* Current Applied Physics, 2013. **13**(2): p. 309-321.
15. H. Osgood, S.V. Devaguptapu, H. Xu, J. Cho, G. Wu, *Transition metal (Fe, Co, Ni, and Mn) oxides for oxygen reduction and evolution bifunctional catalysts in alkaline media.* Nano Today, 2016. **11**(5): p. 601-625.
16. C. Tang, N. Cheng, Z. Pu, w. Xing, X. Sun, *NiSe Nanowire Film Supported on Nickel Foam: An Efficient and Stable 3D Bifunctional Electrode for Full Water Splitting.* Angew Chem Int Ed Engl, 2015. **54**(32): p. 9351-5.

17. L. Elias, K. Scott, A.C. Hegde, *Electrolytic Synthesis and Characterization of Electrocatalytic Ni-W Alloy.* Journal of Materials Engineering and Performance, 2015. **24**(11): p. 4182-4191.
18. A. Sarapuu, A. Kasikov, T. Laaksonen, K. Kontturi, K. Tammeveski, *Electrochemical reduction of oxygen on thin-film Pt electrodes in acid solutions.* Electrochimica Acta, 2008. **53**(20): p. 5873-5880.
19. Z-Y. LI, S-T. Shi, Q-S. Zhong, C-J. Zhang, C-W. Xu, *Pt-Mn 3 O 4 /C as efficient electrocatalyst for oxygen evolution reaction in water electrolysis.* Electrochimica Acta, 2014. **146**: p. 119-124.
20. C. Xu, L. Ma, J. Li, W. Zhao, Z.Gan, *Synthesis and characterization of novel high-performance composite electrocatalysts for the oxygen evolution in solid polymer electrolyte (SPE) water electrolysis.* International Journal of Hydrogen Energy, 2012. **37**(4): p. 2985-2992.
21. S.H. Ahn, I. Choi, H.Y. Park, S.J. Hwang, S.J. Yoo, E. Cho, H.J. Kim, D. Henkensmeier, S.W. Nam, S.K. KIM, J.H. Jag., *Effect of morphology of electrodeposited Ni catalysts on the behavior of bubbles generated during the oxygen evolution reaction in alkaline water electrolysis.* Chem Commun (Camb), 2013. **49**(81): p. 9323-5.
22. I.M. Sadiek, A.M. Mohammad, M.E. El-Shakre, M.I. Awad, M.S. El-Deab, B.E.Anadouli, *Electrocatalytic Evolution of Oxygen Gas at Cobalt Oxide Nanoparticles Modified Electrodes.* International Journal of electrochemical science, 2012. **7**(4): p. 3350-3361.
23. S. Seetharaman, R. Balaji, K. Ramya, K.S. Dhathathreyan, M. Velan , *Electrochemical behaviour of nickel-based electrodes for oxygen evolution reaction in alkaline water electrolysis.* Ionics, 2013. **20**(5): p. 713-720.
24. X. Li, F.C. Walsh, D. Pletcher, *Nickel based electrocatalysts for oxygen evolution in high current density, alkaline water electrolysers.* Phys Chem Chem Phys, 2011. **13**(3): p. 1162-7.
25. C. Kjartansdóttir, M. Caspersen, S. Egelund, P. Moller, *Electrochemical investigation of surface area effects on PVD Al-Ni as electrocatalyst for alkaline water electrolysis.* Electrochimica Acta, 2014. **142**: p. 324-335.
26. V. Rashkova, S. Kitova, I. Konstantinov, T. Vitanov, *Vacuum evaporated thin films of mixed cobalt and nickel oxides as electrocatalyst for oxygen evolution and reduction.* Electrochimica Acta, 2002. **47**: p. 1555-1560.
27. J. Kubisztal, A. Budniok, *Study of the oxygen evolution reaction on nickel-based composite coatings in alkaline media.* International Journal of Hydrogen Energy, 2008. **33**(17): p. 4488-4494.

28. J. Lee, S. Langer, *Electrochemical sulphur dioxide oxidation with platinum-aluminum electrocatalysts.* Journal of applied electrochemistry, 1995. **25**(4): p. 353-357.
29. M.Z. Iqbal, R.J. Kriek, *Silver/Nickel Oxide (Ag/NiO) Nanocomposites Produced Via a Citrate Sol-Gel Route as Electrocatalyst for the Oxygen Evolution Reaction (OER) in Alkaline Medium.* Electrocatalysis, 2018. **9**(3): p. 279-286.
30. Y. Cheng, *Advances in electrocatalysts for oxygen evolution reaction of water electrolysis-from metal oxides to carbon nanotubes.* Progress in natural science: materials international, 2015. **25**(6): p. 545-553.
31. M.S. Burke, L.J. Enman, A.S. Batchellor, S. Zou, S.W. Boettcher, *Cobalt-iron (oxy)hydroxide oxygen evolution electrocatalysts: the role of structure and composition on activity, stability, and mechanism.* J Am Chem Soc, 2015. **137**(10): p. 3638-48.
32. M.E.G. Lyons, M.P. Brandon, *A comparative study of the oxygen evolution reaction on oxidised nickel, cobalt and iron electrodes in base.* Journal of Electroanalytical Chemistry, 2010. **641**(1-2): p. 119-130.
33. H.Y. Su, Y. Gorlin, I.C. Man, F. Calle-Vallejo, J.K. Norskov, T.F. Jaramillo, J. Rossmeisl, *Identifying active surface phases for metal oxide electrocatalysts: a study of manganese oxide bi-functional catalysts for oxygen reduction and water oxidation catalysis.* Phys Chem Chem Phys, 2012. **14**(40): p. 14010-22.
34. D.M. Jang, I.H. Kwak, E.L. Kwon, C.S. Jung, H.S. Im, K. Park, J. Park, *Transition-Metal Doping of Oxide Nanocrystals for Enhanced Catalytic Oxygen Evolution.* The Journal of Physical Chemistry C, 2015. **119**(4): p. 1921-1927.
35. R. Ray, *Fine grained sputtering targets of cobalt and nickel base alloys made via casting in metal molds followed by hot forging and annealing and methods of making same*. 2005, Google Patents.
36. A. Kinbara, E.K., I. Kondo, *FUndamentals of plasma and sputtering processes.* 1998. **51**(4): p. 475-478.
37. D.E.Hall, *Alkaline Water Electrolysis Anode Materials.* Journal of the electrochemical society, 1985.
38. S. Jung, C.C.L. Charles, I.M. Ferrer, J.C. Peters, T.F. Jaramilo, *Benchmarking nanoparticulate metal oxide electrocatalysts for the alkaline water oxidation reaction.* Journal of Materials Chemistry A, 2016. **4**(8): p. 3068-3076.
39. C.J. Warren, R.C. Haushalter, L. Matsiev, *Combinatorial electrochemical deposition and testing system*. 2004, Google Patents.
40. P. Strasser, Q. Fan, M. Devenney, W. H. Weinberg, *High Throughput Experimental and Theoretical Predictive Screening of Materials.* J. Phys. Chem., 2003. **107**: p. 11013-11021.

41. A. Falch, V. Lates, R.J. Kriek, *Combinatorial Plasma Sputtering of PtxPdy Thin Film Electrocatalysts for Aqueous SO2 Electro-oxidation.* Electrocatalysis, 2015. **6**(3): p. 322-330.
42. J.S. Cooper, P.J. McGinn, *Combinatorial screening of thin film electrocatalysts for a direct methanol fuel cell anode.* Journal of power sources, 2006. **163**(1): p. 330-338.
43. M. Kopanica, F. Vydra, *Voltammetry with disc electrodes and its analytical application: II. Anodic stripping voltammetry of trace concentrations of silver and copper employing a glassy carbon electrode.* Journal of Electroanalytical Chemistry and Interfacial Electrochemistry, 1971. **31**(1): p. 175-181.
44. P. Chen, L-K. Wang, G. Wang, M-R. Gao, J. Ge, W-J. Yuan, Y-H. Shen, A.J. Xie, S-H. Yu, *Nitrogen-doped nanoporous carbon nanosheets derived from plant biomass: an efficient catalyst for oxygen reduction reaction.* Energy & Environmental Science, 2014. **7**(12): p. 4095-4103.
45. Y. Cheng, C. Xu, L. Jia, J.D.Gale, L. Zhang, P.K. Shen, S.P. Jiang ,*Pristine carbon nanotubes as non-metal electrocatalysts for oxygen evolution reaction of water splitting.* Applied Catalysis B: Environmental, 2015. **163**: p. 96-104.

4 SUPPLEMENTARY INFORMATION

APPENDIX A: EXPERIMENTAL

SiO_2 wafer

Photolithography

Photolithography as adapted from Strasser et al. and Warren et al. [39, 40] is the method employed in this research to microfabricate a Ti-Au electrical circuit onto a SiO_2 wafer (100mm diameter, 500µm thickness, Microchemicals, Germany) as seen in figure 8. This process included the deposition of a thin, uniform 10µm-thick layer of photoresist (PL177, Microchemicals) onto the wafer and adding more photoresist (Performus dispensing system, EFD Nordson) and then spin coating (Spin 150, SPS Ltd.), thereafter drying at 80°C for 15 min. An image mask of the circuit pattern (Figure 1), is fitted onto the wafer and the exposed ink on the wafer is exposed to 5 mW/cm^2 UV light for 1 min in a UV box (Pluvex 1410, Mega Electronics, UK). Thereafter, the wafer was soaked in a developer solution (RS universal developer) for 20 seconds and rinsed with milliQ water and dried with N_2. Subsequent to the wafer development, vacuum sputtering can be employed for the deposition of the circuit. Deposition of a 106.8-nm-thick Ti-Au layer onto the patterned wafer is done, with the Au being deposited subsequent to the Ti layer. The sputtering conditions of the circuits are as depicted in Table S1. When the sputtering is complete, stripping of the negative part of the circuit is done (removing the sputtered gold metal from the black section of the wafer). The stripping process is performed by soaking the wafer in acetone, bubbling N_2 to cause agitation to speed up the stripping process leaving the sputtered gold on the circuit pattern (Figure S1).

Table S1: Conditions used for sputtering the circuit on the wafer

Vacuum base pressure	5×10^{-7} Torr
Chamber pressure	8 mTorr
Argon flow rate	0.015 L min^{-1}
Ti DC power	50 W for 235 s
Au layer DC power	50 W for 280 s

Combinatorial deposition system

The combinatorial deposition system (Figure 1, PVD products, USA) is used in this study for vacuum sputtering of the electrocatalysts. This system contains four water-cooled magnetron guns each hosting one target metal disk (in this research we only used 3 targets, Pt, Ni and Al) for sputtering purposes. Each metal disk (ACI Alloys, Inc) has a diameter and thickness of 38.1 and 3.2 mm respectively. The opening and closing of the shutters of the magnetrons hosting the target metals is computer-controlled for the sputtering of the targets to take place. These magnetron guns are focussed on the aperture of choice: for the photolithography, the aperture (Figure S1a) a 100-mm-diameter SiO_2 wafer and for the electrocatalysts (Figure S1b) on 4 of 16 GC inserts at once,(Figure S1c and d) on only one square contact pad among a maximum of 64 electrode pads on the SiO_2 wafer and one GC at a time. Before sputtering, the chamber was pumped down to a base pressure of ~5 x 10^{-7} Torr. The four direct current magnetrons have a maximum power rating of 100 W. The composition and thickness of the sputtered thin films are determined from the calibration of the sputtering rate of each metal and was pre-determined [41].

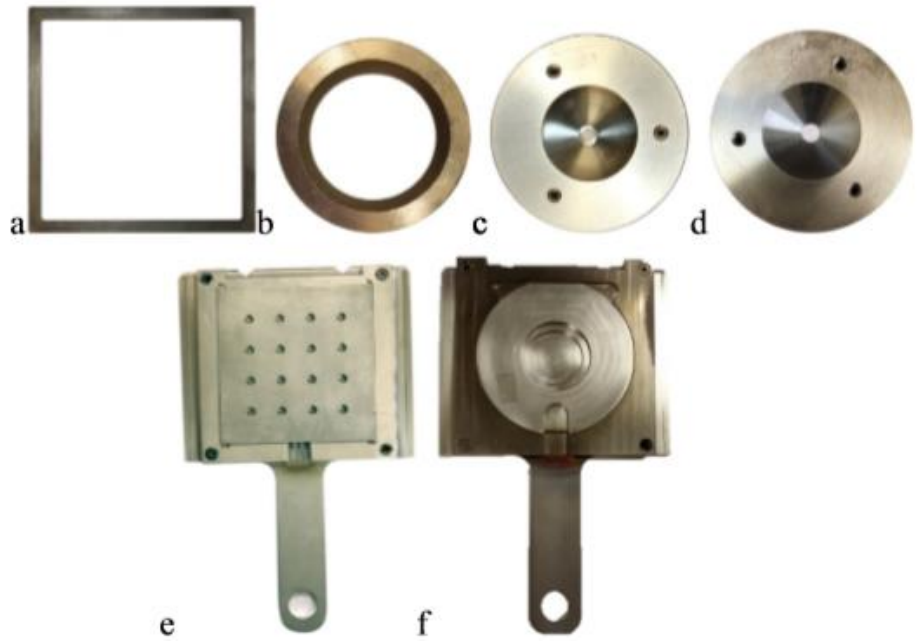

Figure S1. Different apertures employed for sputtering (a) a100-mm- diameter Si-SiO_2 wafer and 16 GC'S at once, (b) 4 of 16 GC' inserts at a time, (c) and (d) one GC electrode or one pad of 64 electrode on a Si-SiO_2 wafer. These apertures are placed on holders (e) for GC electrodes and (f) for Si-SiO_2 wafers [41]

Thin film electrocatalyst deposition on a Wafer

Fifty-four (54) different molar combinations of Pt, Ni and Al, i.e $Pt_xNi_yAl_z$, were individually deposited onto the pads (specifications of pad in Table 1) on the wafer employing the sputtering parameters obtained from the calibration data. Each deposited thin film, representing a specific molar ratio of Pt, Ni and Al, were obtained through co-deposition (Figure 1). Along with the trimetallic combinations, pure Pt, Ni and Al were also sputtered for comparison towards the oxygen evolution reaction. The position of each combination on the wafer were chosen at random as, according to Falch et al., the position of the specific electrocatalyst does not affect the electrical signal of the catalyst [41]. The Au contact pads that were not sputtered with any Pt, Ni or Al were left uncovered (Figure S2)

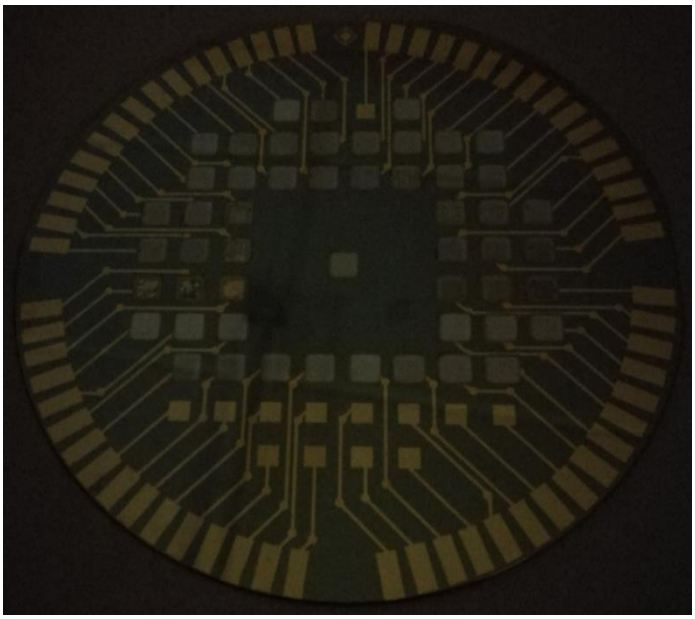

Figure S2. Sputtered wafer with electrocatalysts, the gold pads have no sputtered metals on

Electrochemical cell for screening on wafer

The electrochemical screening of the wafer was done using a designed electrochemical cell (Figure 2), as reported by Cooper et al. [42]. In this cell, the wafer with the sputtered electrocatalysts is placed at the bottom of the double glass body (that is open at the bottom), facing upwards such that they are exposed to the electrolyte solution (300 ml 0.1 M KOH (Merck) O_2-bubbled for 20 min). The O-ring seal incorporated into the cell, seals off the electrolyte solution and the electrocatalysts from the pin pads. The counter electrode is a Pt-coated circular Ti mesh electrode (7 cm diameter) that was placed at about 2.5 cm above and parallel to the wafer. A mercury mercury oxide (Hg-HgO) electrode was used as reference electrode, which was placed above the working electrode through a small opening in the

middle of the counter electrode. A distance of about 1.5 to 2 cm has been chosen between the tip of the reference electrode and the working electrode as to minimize the differences in the uncompensated ohmic resistance between the electrocatalysts. Given the conductivity of the electrolyte and magnitude of the measured currents, the voltage drop across the electrolyte are negligible between the reference electrode and individual working electrode pads [40]. Conditions for electrochemical measurements included a water-jacketed electrochemical cell (300 ml) and a temperature of 25 °C which is externally controlled through a circulation water bath (Julabo F12 ED).

Electrochemical screening on wafer

A high through-put electrochemical technique was employed for the electrochemical screening (LSV) of the combinatorial electrocatalyst array on the wafer. A 64-channel potentiostat (Arbin MStat), connected to the abovementioned electrochemical cell was used for the simultaneous electrochemical measurement of the electrocatalysts. LSV's were performed on the wafer at a scan rate of 5 mV/s within the voltage range of 0.1 V – 0.8 V vs. Hg/HgO. Three LSV repeats were performed with the aim of observing the changes on the activity of the electrocatalyst and the refined xyz-region.

Glassy carbon inserts

Preparation

The glassy carbons (GC, Sigradur G, HTW Germany) used in this study, were polished following the same technique to ensure a reproducible electrochemical surface before the deposition of the thin films [43]. Firstly, the GC's were subjected to 30 polishing cycles (by hand) on a microcloth (Buehler polishing kit) employing diamond paste (1 µm, DP-Paste M, Stuers) and subsequently rinsed with Milli-Q water (specific resistance 18.2 MΩ cm) to ensure that polishing on the second microcloth does not contaminate it with residue from the previous polishing cycle. The second step of the polishing is done using a microcloth with 0.05 µm suspension of deagglomerated alumina (Gamma Micropolish II, Buehler) for another 30 polishing cycles, rinsing with Milli-Q water and drying in air. Lastly the GC's were ultrasonicated in toluene (HipervSolv for HPLC, BDH Laboratory Supplies) for 10 minutes, in ethanol (Merck) for 10 minutes, Milli-Q water for 10 minutes and iso-propanol (Merck) for 10 minutes. The GC's were then dried with N_2 and sealed in a beaker.

Thin film electrocatalyst deposition

The 10 most active electrocatalysts ($Pt_{15}Ni_{80}Al_5$, $Pt_{10}Ni_{55}Al_{35}$, $Pt_{15}Ni_{65}Al_{20}$, $Pt_{35}Ni_{60}Al_5$, $Pt_{25}Ni_{60}Al_{15}$, $Pt_{10}Ni_{60}Al_{30}$, $Pt_{15}Ni_{55}Al_{30}$ $Pt_{15}Ni_{60}Al_{25}$, Pt_5Ni_{95}, Ni_{100}) were deposited on 30 GC's

(each thin film is sputtered in triplet, for repeatability of electrochemical measurements) in the form of thin films (30 nm) using physical vapour deposition. The ratios were chosen based on the refinement runs that were done on the wafer.

Calibration of Hg/HgO electrode

Before the Hg/HgO reference electrode (Radiometer) was used for electrochemical testing, it was first calibrated using a method suggested by Cheng Ping et al. [44]. In a three-electrode setup system, a polished Pt GC was used as the working electrode, a Pt wire as counter electrode, and Hg/HgO as reference electrode. The 0.1 M KOH electrolyte was saturated with high purity H_2 (bubbled H_2 in the electrolyte for 20 minutes). Three LSV scans were conducted at a scan rate of 0.5 $mV.s^{-1}$and the potential at which the current crossed zero was taken as the thermodynamic potential for the hydrogen electrode reactions. The potential was measured as being 0.929V vs. RHE. Using the equation below, the potentials were IR-corrected:

$$E_{IR\ corrected} = E_{App} - IR$$

where R is the ohmic resistance of the cell and I is the current. Employing an impedance measurement technique (ZIR), the uncompensated ohmic resistance of the cell was measured as 41.20 Ω [29].

Electrochemical measurements on GC's

For the electrochemical measurements, linear sweep voltammetry (LSV) and chronopotentiometry (CP) techniques were performed using a conventional three-electrode setup in an electrochemical cell. A platinum spiral wire (Pine Research Instrumentation) was used as counter electrode and the same Hg/HgO (previously calibrated) was used as reference electrode. The working electrodes were the sputtered GC's (geometric area of 0.196 cm^2) with different electrocatalysts ($Pt_xNi_yAl_z$). The working electrode was set up into a rotating disk electrode (RDE) setup (Pine Research instrumentation), which assist in minimising the overpotential caused by the formation of oxygen bubbles at high current densities and it furthermore aids in the mass transport of the active species from the bulk of the solution to the surface of the working electrode [21, 45]. All measurements (current potential curves) were obtained using a WaveDriver 20 Bipotentiostat (Pine Research Instrumentation) with AfterMath software (version 1.25966). All the electrochemical measurements were carried out under the same conditions, in O_2-saturated 0.1 M KOH (Merck, uniVAR), at constant temperature of 25 °C and a rotation rate of 1600 rpm.

The current densities were measured using linear sweep voltammetry (LSV) on the electrocatalysts sputtered on the GC's before and after CP measurements. For each GC, 130 ml of O_2-saturated (10 minutes) 0.1 M KOH was used in the OER region of 0.929 to 2.129 V vs. RHE at a scan rate of 10 mV/s. Three repeats were performed for each electrocatalytic ratio and the mean linear polarisation curve was used.

Chronopotentiometry (CP) was used to test the stability of the electrocatalysts. Each of the 10 electrocatalytic ratios sputtered on the GC's were subjected to a 10 hours CP scan at a constant applied current of 1.96 mA.

Thin film structural characterisation

The structural characterization of the sputtered thin films on the GC's was done before and after the electrochemical measurements employing an Xmax 20 Energy-dispersive X-ray spectroscopy (EDX, Oxford Instruments).

APPENDIX B: CALCULATIONS AND RESULTS

Conversions to RHE

$E_{RHE} = E_{(Hg/HgO)} + 0.929\ V$

0.929 V was the value obtained from the calibration of the Hg/HgO reference electrode.

Calculation of overpotential (η)

1. Plot mA/cm^2 vs. $V_{IR\ corrected}$

   $E_{IR\ corrected} = E_{app} - IR$ $\qquad$ $R = 41.2\ \Omega$

   $= E_{app} - I(41.2\ \Omega)$

2. Get the potential $V_{(RHE)}$ @ $10mA.cm^{-2}$

   $\eta = E_{(RHE)} - E_{eq}$

   For OER: $4OH^- \rightleftharpoons O_2 + 2H_2O + 4e^-$ $\qquad$ $E^o = -0.401\ V$

   Thermodynamic electrode potential for OER is 1.23 V vs. RHE

   Therefore,

   $\eta = E_{(RHE)} - 1.23\ V$

Tafel slopes

The graphs below are the Tafel plots for the electrocatalysts before and after CP testing. These Tafel plots were chosen in the overpotential range 200 - 400 mV vs. RHE.

The Tafel slopes were obtained from the plots of ln j vs. η

slope = $(1 - \alpha)\frac{nF}{RT}$

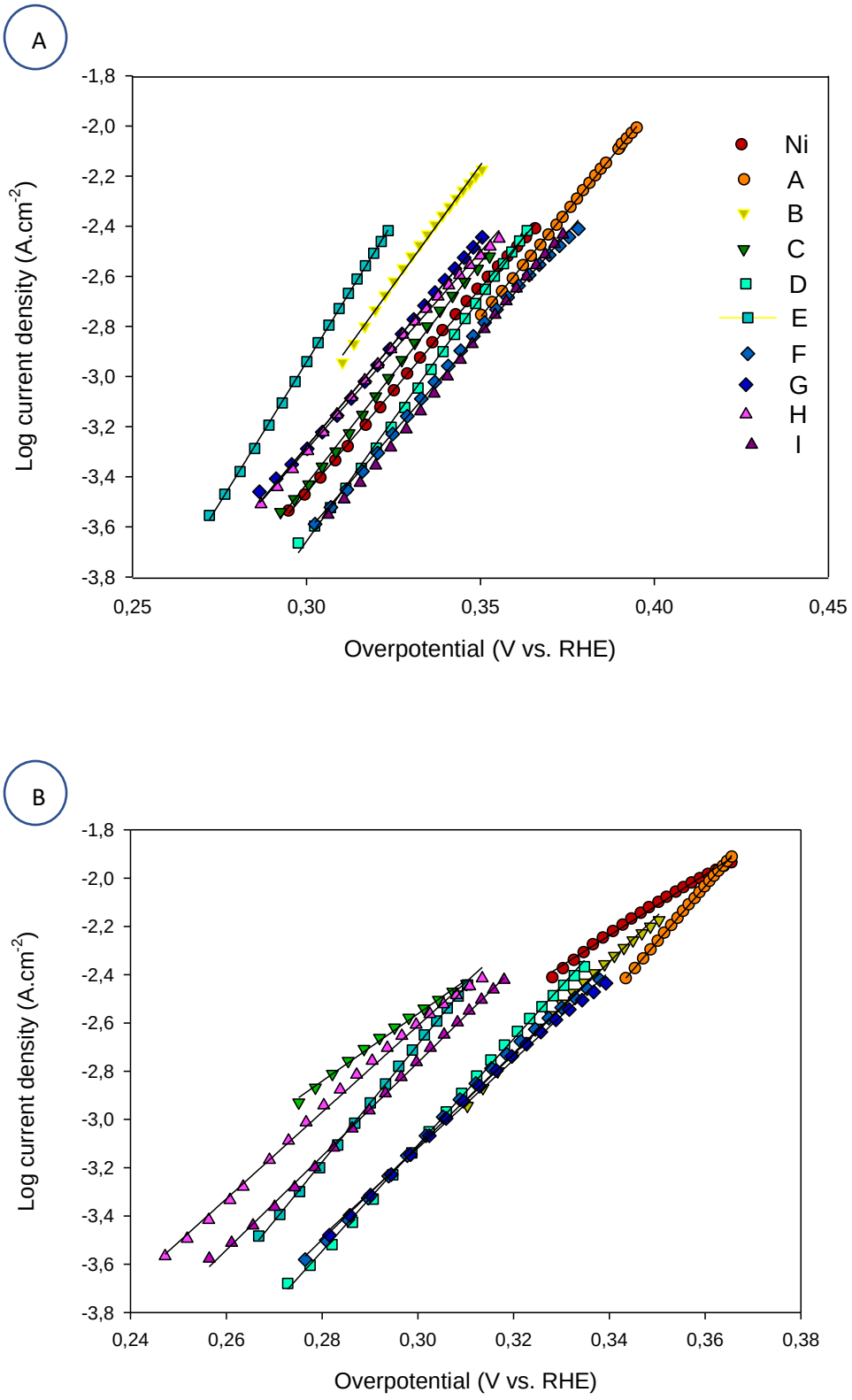

Figure S3. Tafel slopes of the ten best electrocatalysts sputtered on the GC electrodes (a) before CP and (b) after CP

Specific mass activity per Pt and Ni loading

Table S2: Parameters used to calculate the specific mass activities (current density per mass of Pt loading) of the ten best electrocatalysts

Samples	**µgPt (before CP)**	**µg Pt (after CP)**	**Current density @ 1,6 V vs RHE (before CP)**	**Current density @ 1,6 V vs RHE (after CP)**	**$mA.cm^2.ugPt^{-1}$ (before CP)**	**$mA.cm^2.ugPt^{-1}$ (after CP)**
Pt	9.46	-	0,04	-	0,00	-
A	0,437	0,437	10,96	22,24	25,08	50,88
B	1,928	1,896	8,24	14,96	4,28	7,89
C	1,317	0,463	3,57	13,54	2,71	29,25
D	0,128	0,11	5,345	15,33	41,76	139,40
E	0,702	1,546	16,39	23,33	23,34	15,09
F	0,978	0,521	2,99	11,09	3,06	21,30
G	7,617	7,58	4,96	8,56	0,65	1,13
H	1,317	0,964	2,14	12,20	1,63	12,66
I	0,406	0,724	5,03	18,31	12,39	25,29

Table S3: Parameters used to calculate the specific mass activities (current density per mass of Ni loading) of the ten best electrocatalysts

Samples	**µg Ni (before CP)**	**µg Ni (after CP)**	**Current density @ 1,6 V vs RHE (before CP)**	**Current density @ 1,6 V vs RHE (after CP)**	**$mA.cm^2.ugNi^{-1}$ (before CP)**	**$mA.cm^2.ugNi^{-1}$ (after CP)**
Ni	8,982	8,982	4,86	12,89	0,54	1,43
A	2,295	2,295	10,96	22,24	4,78	9,69
B	4,668	3,558	8,24	14,96	1,77	4,21
C	2,287	0,79	3,57	13,54	1,56	17,14
D	0,344	0,344	5,34	15,33	15,54	44,58
E	1,27	2,249	16,39	23,33	12,90	10,37
F	1,007	0,401	2,99	11,09	2,97	27,68
G	6,082	5,879	4,96	8,56	0,82	1,46
H	2,747	2,629	2,14	12,20	0,78	4,64
I	0,651	1,827	5,03	18,31	7,73	10,02